

**Sebastian Rohm, BSc**

# **Thin Cellulose Films as Model Systems for Paper-Fibres**

**MASTER THESIS**

For obtaining the academic degree  
Diplom-Ingenieur

Master Programme of  
Technical Physics



**Graz University of Technology**

Supervisor:

Ao.Univ.-Prof. Mag. Dr.rer.nat Robert Schennach

Institute of Solid State Physics

Graz, January 2013

Deutsche Fassung:  
Beschluss der Curricula-Kommission für Bachelor-, Master- und Diplomstudien vom 10.11.2008  
Genehmigung des Senates am 1.12.2008

## EIDESSTÄTLICHE ERKLÄRUNG

Ich erkläre an Eides statt, dass ich die vorliegende Arbeit selbstständig verfasst, andere als die angegebenen Quellen/Hilfsmittel nicht benutzt, und die den benutzten Quellen wörtlich und inhaltlich entnommene Stellen als solche kenntlich gemacht habe.

Graz, am .....

.....  
(Unterschrift)

Englische Fassung:

## STATUTORY DECLARATION

I declare that I have authored this thesis independently, that I have not used other than the declared sources / resources, and that I have explicitly marked all material which has been quoted either literally or by content from the used sources.

.....  
date

.....  
(signature)

# Contents

<b>1</b>	<b>Introduction</b>	<b>1</b>
1.1	Motivation . . . . .	1
1.2	Paper–Historic development and importance today . . . . .	1
1.3	Woodpulp . . . . .	2
1.3.1	Cell wall . . . . .	2
1.3.2	Microfibril . . . . .	3
1.3.3	Cellulose . . . . .	4
1.3.4	Hemicellulose-Xylan . . . . .	4
1.4	Model system . . . . .	5
1.4.1	Introduction . . . . .	5
1.4.2	Model system for fibre-fibre bonding . . . . .	5
<b>2</b>	<b>Test execution</b>	<b>9</b>
2.1	Film production . . . . .	9
2.2	Swelling and drying . . . . .	10
2.3	Tensile tests . . . . .	11
2.3.1	Calculation of the data . . . . .	13
2.3.2	Statistical analysis . . . . .	14
2.4	Task . . . . .	15
2.5	Nanoindentation . . . . .	15
<b>3</b>	<b>Measurements and results</b>	<b>18</b>
3.1	Calibration . . . . .	18
3.2	Cellulosefilm . . . . .	19
3.2.1	Infrared spectroscopy . . . . .	19
3.2.2	AFM examination of the films . . . . .	24
3.3	Cellulose swelled in distilled water . . . . .	25
3.3.1	Reasons for experimental non-validation of tensile tests . . . . .	26
3.3.2	Calculation of the data . . . . .	28
3.3.3	Nanoindentation . . . . .	31
3.3.4	Roughness-Investigation . . . . .	32
3.4	Cellulose swelled in ionic water . . . . .	33
3.4.1	Calculation of the data . . . . .	34
3.4.2	Comparison to cellulose swelled in distilled water . . . . .	37
3.5	Xylan . . . . .	40
3.5.1	Production of the xylan films . . . . .	40
3.5.2	Results . . . . .	43
3.5.3	Calculation of the data . . . . .	44
3.5.4	Nanoindentation . . . . .	46
3.5.5	Comparison to cellulose . . . . .	47

3.6	Cellulose-Xylan . . . . .	48
3.6.1	Calculation . . . . .	48
3.6.2	Comparison of the results obtained to cellulose and xylan . . . . .	51
3.7	Xylan with dimethyl sulfoxide (DMSO) . . . . .	52
3.7.1	Calculation . . . . .	53
3.7.2	Comparison of the results to xylan . . . . .	54
3.8	Xylan swelled in ionic water . . . . .	55
3.8.1	Calculation . . . . .	57
3.8.2	Comparison with other settings . . . . .	58
<b>4</b>	<b>Summary</b>	<b>61</b>
4.1	Outlook . . . . .	63
	<b>Bibliography</b>	<b>64</b>
	<b>List of figures</b>	<b>67</b>
	<b>List of tables</b>	<b>70</b>
<b>A</b>	<b>Analysis with Matlab</b>	<b>72</b>

# Abstract

This master thesis was carried out at Graz University of Technology within the framework of the Christian Doppler Laboratory for Surface Chemical and Physical Fundamentals of Paper Strength. The main task is the investigation of fibre-fibre bonding in paper. For this purpose a model system based on thin cellulose or hemicellulose model films was developed. To simulate the bonding process, these films are put together and dried, after swelling in distilled or ionic water. These samples then undergo a tensile test, whereby the bonding energy and the maximum strength are of great interest. For additional informations the samples are investigated by nanoindentation, infrared spectroscopy and atomic force microscopy.

The cellulose films are produced by first spincoating trimethylsily cellulose (TMSC) (solved into Toluol) on a silicon substrate which then is transformed to cellulose by hydrolysis. To investigate the bonding influence of hemicellulose molecules, xylan solved in dimethyl sulfoxide (DMSO) is spincoated on the existing cellulose films. For swelling these wafers are laid into distilled water. To measure ionic influences some wafers are also swelled in water containing 0.1mol/l  $\text{CaCl}_2$ . After that two cellulose or xylan surfaces are laid on each other like a sandwich and put into a dryer. While the water evaporates, physical bonds are forming between the film surfaces. After 4 hours of drying the thin films are joint and tensile tests can be performed. The advantage of this method is, that only physical bonds like Coulomb interactions, Van-Der-Waals- and hydrogenbonds are contributing. The hardness of the produced films before and after swelling is investigated with the nanoindentation technique to get an idea of the specific swelling behaviour. For that, a three-sided pyramid is pressed with a specific force into the film while the penetration depth is measured. In addition the roughness of the films before and after the strength tests are examined with an atomic force microscope, to find out more about the area in molecular contact.

During the course of the work 6 different settings were investigated and compared to each other. To minimize possible errors, at least 14 valid experiments and at least 2 independent test series for each configuration were performed. The individual data, except of one, are normal distributed and that is why they can be compared by a statistical t-test. Swelling Cellulose in ionic water leads to a significant reduction in the bonding strength. The reason for this reduction is mainly due to the increase in hardness and, therefore, due to the reduction of the area in molecular contact. Despite better swelling properties, there is no significant increase in strength or bonding energy for the xylan samples compared to the cellulose. The rougher surface of the spincoated xylan films, and therefore, the smaller molecular contact area between the samples, is the most significant reason for that. However, swelling them in ionic water leads to a strong increase in strength and bonding energy. Hereby the positiv charged  $\text{Ca}^{2+}$ -Ions can attach to the negativ acide groups of the xylan and strong coulomb interactions are formed. Furthermore, these interactions completely cancel out the negative effect of the rougher film surface. Also, mixed samples (CelluloseXylan) and xylan samples with DMSO supported swelling is leading to an increase in both categories.

# Kurzfassung

Diese Masterarbeit wurde auf der Technischen Universität Graz im Rahmen des Christian Doppler Labors für oberflächen-chemische und physikalische Grundlagen der Papierfestigkeit verfasst. Das Ziel der Arbeit war ein besseres Verständnis der Faser-Faser Bindung und dessen Mechanismen in Papier. Dazu wurde ein Model System basierend auf dünnen Cellulose beziehungsweise Hemicellulosefilmen entwickelt. Durch Trocknung von zwei aufeinander gelegten gequellten Proben kann die Faserbindung in Papier gut simuliert werden. Die Bindungsenergie und die maximale Zugfestigkeit dieser Proben wurden dann mithilfe eines Zugversuches ermittelt. Zusätzlich werden die Filme mittels der Infrarotspektroskopie, dem Rasterkraftmikroskop und der sogenannten Nanoidentationmethode untersucht.

Die Cellulosefilme werden durch Spincoating von (in Toluol gelöstem) Trimethylsilyl Cellulose (TMSC) auf Siliziumsubstrate und anschließender Hydrolyse zu Cellulose hergestellt. Um Untersuchungen an Hemicellulosemolekülen durchführen zu können, wird Xylan, gelöst in Dimethylsulfoxid, mit der gleichen Methode auf die bereits hergestellten Celluloseschichten aufgebracht. Diese Proben werden durch einer Lagerung in destilliertem Wasser, beziehungsweise um den Einfluss von ionischen Bestandteilen untersuchen zu können, in salzhaltigem Wasser (0.1mol/l  $\text{CaCl}_2$ ) gequellt. Anschließend werden zwei Filme aufeinander gelegt und in einem Blatztrockner getrocknet. Während dieses Trocknungsprozesses kommt es zu einer Ausbildung von physikalischen Bindungen. Nach einer Trocknungszeit von 4 Stunden werden die Proben, mithilfe eines modifizierten Power Rheometers, einem Zugversuch unterzogen. Der Vorteil dieses Modellsystems liegt darin, dass nur Coulombwechselwirkungen, Van-der-Waals- und Wasserstoffbrückenbindungen zur Gesamtbindung beitragen. Durch Messen der Härte vor und nach der Lagerung im Wasser kann das Quellverhalten der Probe untersucht werden. Dabei wird eine genau definierte 3-seitige Pyramide mit einer vorgegebenen Kraft in die Probe gedrückt und die Eindringtiefe gemessen. Um eine Abschätzung über die Fläche im molekularen Kontakt zu bekommen, wird weiters die Rauheit einer Probe vor und nach dem Zugversuch mithilfe eines Rasterkraftmikroskops bestimmt.

Ingesamt wurden Proben in 6 verschiedenen Konfigurationen untersucht und miteinander verglichen. Um mögliche Fehlerquellen zu minimieren, wurden jeweils mindestens 14 gültige Zugversuche in mindestens zwei unabhängigen Versuchsreihen durchgeführt. Da, ausgenommen der in Salzwasser gequellten Xylanproben, alle Datensätze normalverteilt sind, können sie einem Signifikanztest (t-Test) unterzogen werden. Durch Quellen in salzhaltigem Wasser kommt es für Celluloseproben zu einer signifikanten Reduktion der maximalen Zugfestigkeit. Der Hauptgrund dafür ist die Zunahme an Härte im gequellten Zustand. Obwohl Xylan ein besseres Quellverhalten als Cellulose aufweist, nimmt für in destilliertem Wasser gequellte Proben weder die maximale Zugfestigkeit noch die Bindungsenergie signifikant zu. Die größere Oberflächenrauigkeit der Xylanfilme führt dazu, dass die Fläche im molekularen Kontakt nahezu ident bleibt. Durch das Quellen in  $\text{CaCl}_2$ -haltigem Wasser kommt es jedoch für Xylan zu einer erheblichen Festigungssteigerung. Dabei entstehen zwischen den  $\text{Ca}^{2+}$ -Kationen und den negativen Säuregruppen des Xylans starke anziehende Coulomb Kräfte. Versuche mit Mischproben (eine Seite Xylan, die andere Cellulose) und Xylan Proben die mit DMSO Unterstützung gequellt werden, führt, im Vergleich zu reinen Xylan beziehungsweise Cellulose-Proben, zu einer Festigkeitssteigerung.

# Chapter 1

## Introduction

### 1.1 Motivation

Paper is one of the most common basic materials in today's life. From everyday products like newspapers, books, notepads or toilet paper, to paper filters for vacuum cleaners or paper as an isolator in condensators, this material is omnipresent. Nevertheless, the physical and chemical fundamentals in the molecular level are still not very well understood. Therefore, a lot of the improvements and innovations nowadays are based on the "Trial and error"-principle.

That is one of the reasons that the Institute of Solid State Physics, the Institute for Paper-, Pulp- and Fibre Technology at the TU Graz, the Institute of Physics at the Montan University in Leoben and industrial partners formed the "Christian Doppler Laboratory for Surface Chemical and Physical Fundamentals of Paper Strength". One of the main aims of this organization is to understand fibre-fibre-bonding, which should lead to a better understanding of paper.

Paper mainly consists of a network of cellulose fibres. Since cellulose fibres are biological materials, not one fibre resembles another. The investigation is very complex and the results can be very diverging. Therefore, a model system which represents an ideal system and is based on reproducible amorphous thin cellulose film layers, is developed. The geometries are simple and only fundamental bonding mechanism, like Van-der-Waal- and hydrogen bonds are contributing. Coulomb-bonding can be controlled by adding defined charged species to the initially electrostatically neutral surfaces. This simplified system yields the possibility to obtain reproducible results to understand the fundamentals of fibre-fibre bonding in paper.

The main aim of this work is to perform tensile tests with these films and investigate, how the behaviour of the films is changed, when different influences, like hemicellulose, are added.

### 1.2 Paper—Historic development and importance today

The invention of paper, respectively the manufacturing of paper, is attributed to a Chinese courtier named Ts'ai Lun around AD 105, although there might have been papermaking in China earlier than this date [1]. In the 10th century the Muslims, who lived in modern Portugal, Spain and Sicily, brought the craft of papermaking to Europe. The most common sources were recycled fibres from used hemp-, linen- or cotton-textiles called rags. Since the demand for paper rose rapidly in the 19th century, it was essential to find a substitute-resource. In 1844 Friedrich Gottlob, a German inventor, invented the so called wood-cut machine which could produce pulp (so called groundwood pulp) out of wood [2]. Since paper, manufactured out of groundwood pulp, contains all components of wood, it possesses a lot of unwanted behaviour (e.g. yellowing, because of lignin). Therefore, chemical processes to improve pulp quickly followed. One of the most important one is the sulfate- or Kraft-process. It uses a mixture of

sodium hydroxide and sodium sulfide, better known as white liquor to break the bonds between the lignin and the cellulose [3]. Nowadays the paper- and fibre-industry is an important part of the world economy and produces around 393 Mio. t of pulp per year. Alone in Austria over 8000 people are working in this branch (Status 2010) [4].

## 1.3 Woodpulp

To get an idea of the behaviour of paper, it is inevitable to understand the chemical composition and the structure of wood. The three main elements Carbon (C), Oxygen (O) and Hydrogen (H) form makromolecules, which are the main cell wall components: Cellulose, hemicellulose and lignin. The composition of hemicellulose and lignin differs with the type of wood, while cellulose is quite uniform in all woods [5].

### 1.3.1 Cell wall

The microscopic structure of wood, the cell wall consists of several different layers (Figure 1.1). These layers differ in their chemical composition and in the different orientation of the structural elements. The middle lamella (ML), which is in principle free of cellulose, glues the different cells together. The outer layer of the cell is called primary layer (P) and consists of a loose accumulation of microfibrils with random orientation. Since plants are growing, cells need to expand, that is why both the middle lamella and the primary wall are extensible. The next inner layer of the cell is the secondary wall, which is usually subdivided in three sub-layers (S1,S2,S3). In the fine layer S1 ( $0.12-0.35\mu m$ ) the fibrils show counter-running helical slopes. It is followed by the thickest wall S2 ( $2-5\mu m$ ). Therefore, S2 is dominating the physical and mechanical properties of the cell. The microfibril angle (MFA) depending on the woodcell varies between  $10-30^\circ$ . S3 is sometimes barely recognizable, with a thickness of about  $0.10-0.14\mu m$  and has a MFA between  $60-90^\circ$ . According to [6] the varying fibril concentrations and angles of the layers lead to a mechanical locking effect, which is increasing the stiffness of the cell. The inner most part of the cell is the lumen, which is a void space and because of that does not have any structure. If the wood is waterlogged, this space is filled with water and that is why it is a critical component of the wood cell [7].

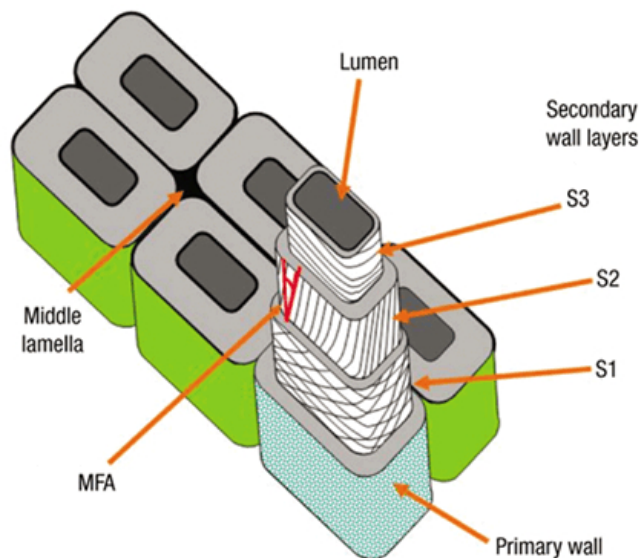


Figure 1.1: Model of the cell wall structure. The grey lines in the secondary wall layers represent idealized cellulose microfibrils [8].

### 1.3.2 Microfibril

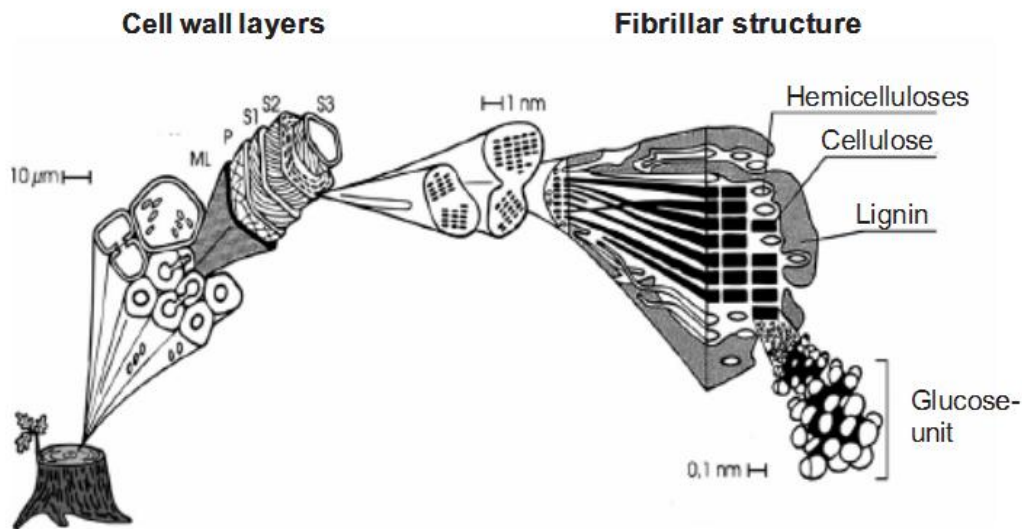


Figure 1.2: A schematic description of the microfibril. From the left to the right: Tree trunk, tissue structure, Cell walls, macrofibrils, microfibrils and molecules. [5]

The tree trunk (Figure 1.2, left) is built up by cell walls (Chapter 1.3.1), which are embedded in a so called tissue structure. The cell walls, moreover are made up of macrofibrils (Figure 1.2, middle). These fibrils are an accumulation of microfibrils with diameters of 10-35nm, enclosed by lignin and hemicellulose. The microfibrils framework consists of cellulose molecules, which form, because of regular hydrogen bonds (Chapter 1.4.2), elementary fibrils. These cellulose regions are wrapped in by shorter hemicellulose chains and at the edge of the fibres, lignin is deposited (Figure 1.2, right). Hemicellulose and lignin have an amorphous structure, the cellulose structure however is partly crystalline. These crystalline regions are called micelles.

### 1.3.3 Cellulose

Cellulose is one of the most abundant resources of the world. It is part of all plants, from trees to primitive organisms like bacteria or sea weeds. Anhydroglucose units (short: AGU) are linked by  $\beta$ -1,4-glycosidic bonds, to form a strictly linear homopolymer chain, the cellulose (Figure 1.3). Two anhydroglucose units form the repeating unit, the so called cellobiose. At the positions 2, 3 and 6 hydroxy groups are attached, which are free for reactions. Each molecule has a reducing (Hydroxy-group at C1) and a non-reducing end (Hydroxy-group at C4). The average degree of polymerisation (DP), which is the number of anhydroglucose units, is between 3.000 and 15.000 depending on the source [5].

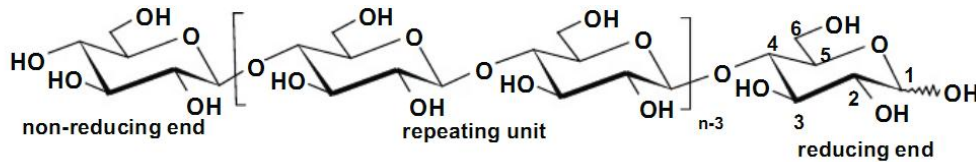


Figure 1.3: Structure of a cellulose molecule after [5]

The supramolecular structure of the cellulose makes cellulose a very complicated material, since it has the ability to form different types of hydrogen bonds (Chapter 1.4.2).

### 1.3.4 Hemicellulose-Xylan

Hemicelluloses are long carbohydrate molecules formed by repeated monomer units (Polysaccharid). Since they usually consists of more than one monosaccharide, they are heteropolysaccharides. Furthermore, they are mostly branched and have lower molecular masses than cellulose with a DP (Degree of Polymerization) of around 50-200 [5].

In this work the most common type of hemicellulose, xylan is used. Depending on the source, xylan exists in several different structural varieties (examples for soft- and hardwood in figure 3.27). As a backbone, xylan, extracted out of wood, usually possesses  $\beta$ -1,4 linked xylose units, which are substituted in irregular intervals by different sidegroups. Common sidegroups are the 4-O-methyl-D-glucuronic acid (1), L-arabinofuranose (2) or O-acetylgroups [9].

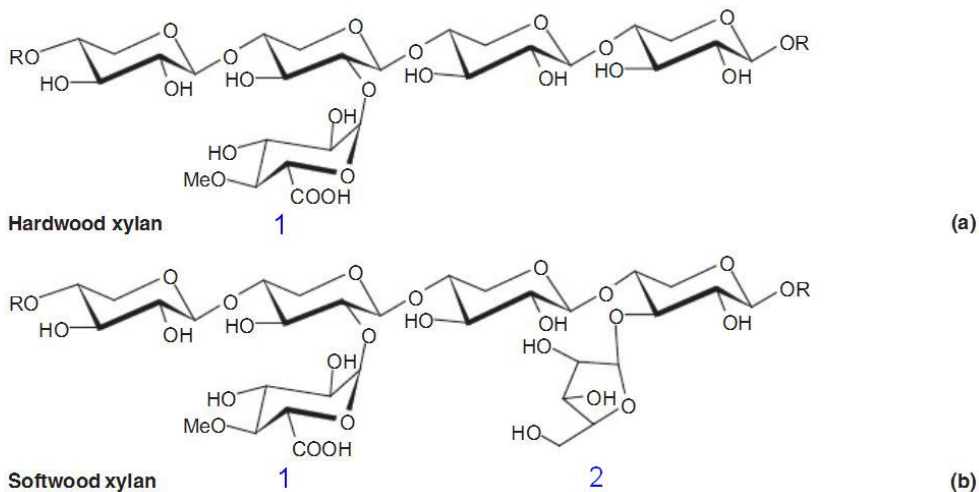


Figure 1.4: Molecular structure of xylan for soft- and hardwood [5]

## 1.4 Model system

### 1.4.1 Introduction

Model systems, like the Bohr model of the atom or the Gaussian-chain model of a polymer, are one of the most important instruments to understand complex scientific systems [10].

That is why model cellulose surfaces are starting to play a significant role in investigating the physical and chemical fundamentals of cellulose. Spincoated cellulose films, as used in this work, have already been used in multiple kinds of investigations like:

- Determining the Hamaker constant of cellulose by measuring the attractive van-der-Waals forces of cellulose surfaces with an atomic force microscope in aqueous conditions [11].
- The moisture-related swelling, e.g. by measuring the film thickness in dependency on the humidity [12].
- Studying the adsorption of different materials, like polyelectrolytes or surfactants [13].

More cellulose model film investigations are illustrated in [13].

### 1.4.2 Model system for fibre-fibre bonding

Paper strength mainly consists of three properties: The network, the single-fibre-strength and the strength of the fibre-fibre bonding.

Fibre-fibre bonding has been already analysed over many years, but still hardly any method delivers quantitative results. Many different influences, like the bonding area, the bonding angle, the roughness of the fibres, swelling properties and many more are making the investigation extremely complex. Furthermore, in total 5 different bonding mechanisms are contributing:

- Mechanical interlocking
- Interdiffusion
- Van-der-Waals bonding,
- Hydrogen bonding
- Coulomb interaction

To understand the contribution of the last 3 points, the model system illustrated in Figure 1.5 is developed.

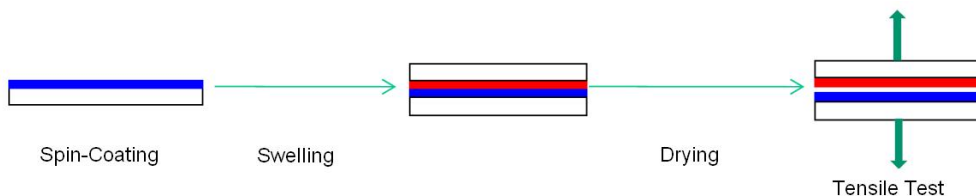


Figure 1.5: Schematic image of the model system and the test procedure.

First thin amorphous [14] cellulose or hemicellulose films are spincoated on a silicon substrate. After swelling them in water, two samples are put together like a sandwich and dried. During drying the bonds are formed and then a tensile test is performed, which measures the maximum force and the energy needed to rip the two layers apart (Figure 1.5). By spincoating these films

always in the exact same way influences, like the roughness of the films, the swelling properties and the bonding area, can be controlled or measured.

Since the two films surfaces, at least in theory, are perfectly plain, mechanical interlocking can be neglected (Figure 1.6). Interdiffusion is the diffusion of cellulose/hemicellulose molecules from one wet fibre to another fibre. The formed bond is mainly because of interactions between the diffused molecule and molecules of the other fibre. These interactions are again hydrogen-, Van der Waals- and Coulomb-bonding.

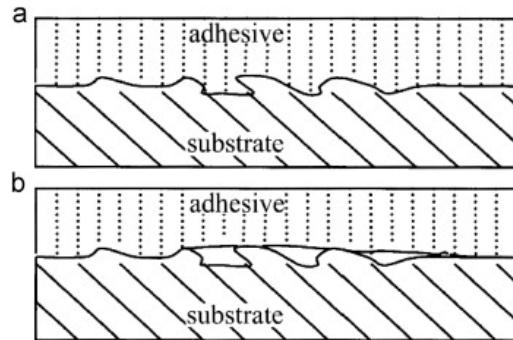


Figure 1.6: Example for good (a) and bad (b) mechanical interlocking [15].

### Van-der-Waals bonds

Van-der-Waals bonding occurs between all kinds of atoms or molecules. One of the main reason is the charge shifting of the electrons in respect to the nucleus in the atoms or molecules. That means the bonding strength depends on the molecule contact surface between the films or, for paper, between the fibres and increases with the size of it. In theory the Van-der-Waals contribution to the fibre-fibre bonding would add up to an energy of  $2.4 \cdot 10^{-22} \frac{kJ}{nm^2}$  [16].

### Hydrogen bonds

In cellulose the OH groups can form either intramolecular (within the same chain) or intermolecular (between different chains) hydrogen bonds. These bonds are illustrated by dotted lines in Figure 1.7. Horizontal bonds are intramolecular, vertical dotted lines indicate intermolecular bonds. Intramolecular hydrogen bonds are of great relevance to chain stiffness and conformation. Intermolecular bonds on the other hand are important for the formation of the supramolecular structure, like fibrils and crystalline domains. In hemicellulose also the acid function (Chapter 1.3.4) is attributing to the hydrogen bonding. The bonding, as for Van-der-Waals, depends on the size of the molecular contact area and in addition on the number of OH groups, or acid functions in this area. The calculated hydrogen bond contribution to pure cellulose fibre-fibre bonding is  $9.1 \cdot 10^{-23} \frac{kJ}{nm^2}$  [16].

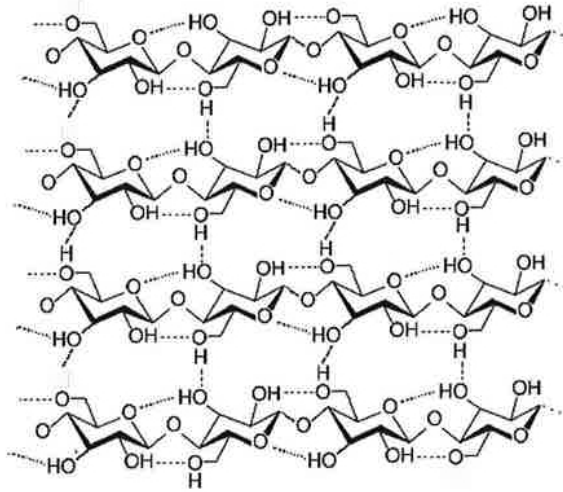
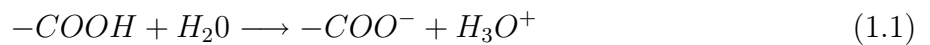


Figure 1.7: Intra- and intermolecular hydrogen bonds in a cellulose molecule network. The bonds are marked with dotted lines [14].

### Coulomb bonds

The Coulomb law describes the interaction between electrical charges (Figure 1.8). Since no charged species exist in cellulose molecules, adding cations or anions should not, in theory, make a big difference.

Hemicellulose molecules on the other hand possess acid sidegroups (Chapter 1.3.4). During swelling these sidegroups react with water to:



To the water added cations (Positive charge), like calcium ( $Ca^{2+}$ ), or sodium ( $Na^+$ ), are forming attractive Coulomb bonds with these now negative charged sidegroups. According to [17], the bonding energy could increase with maximal  $1 \cdot 10^{-21} \frac{kJ}{nm^2}$  depending on the amount of acid groups on the surface and of the amount of cations added.

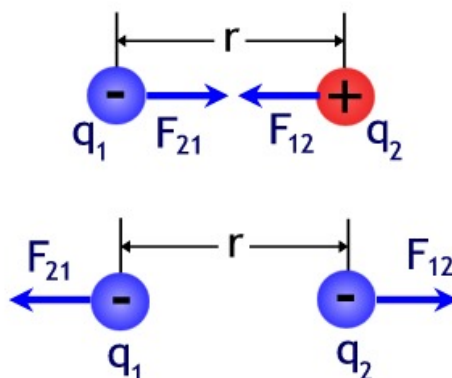


Figure 1.8: Explanation of the Coulomb interaction [18]. Opposite charged particles attract each other (top), same charged particles repel each other (bottom).

## Swelling

Swelling is due to the break-up of the hydrogen bonds by water. That is why swelled fibres and also swelled films experience a strong reduction of the penetration hardness compared to dried fibres. Because of attractive capillary bridges, caused by the water at the interface between the two films, the swollen and hence softer films get pulled closer together. That leads to a higher contact surface and to the connection of the films [19]. Furthermore, because of the additional water, the swelling leads to an increase of the thickness of the films, up to a ratio of  $\frac{d_{max}}{d_0} = 1.7$  [12]. Since the spincoated surfaces are, in reality, not perfectly flat but have a defined roughness, the swelling of the films is very important for the resulting contact surface and, therefore, for the resulting bonding strength.

# Chapter 2

## Test execution

### 2.1 Film production

#### Silicon substrates

$20,0 \times 20,0 \pm 0,1\text{mm}$  silicon wafers are used as substrate material for the cellulose-films. The thickness is  $675 \pm 20\mu\text{m}$  and they are single-side polished.

#### Pre-preparation

First the substrates are cleaned with isopropanol by using a dustfree rag. Afterwards, to get rid of organic contaminations, the wafers are placed in the oxygen-plasma-etching machine, where oxygen plasma reacts with the contaminations (e.g.:  $C + 2O \rightarrow CO_2$ ). The products of the reactants are gaseous and get pumped off by the vacuum pump. Used is a “Plasma system FEMTO timer” by electronic-diener. The duration of the etching process is 90s with maximum etching power at a vapour pressure of  $\sim 0.2\text{mbar}$ . Finally, to get rid of any dustparticles, the substrates get cleaned with a  $CO_2$  spray bottle.

#### Spincoating

To create uniform thin films, spincoating is used. The main steps are illustrated in Figure 2.1. The substrate is put on the rotating plate and gets sucked on it, by a vacuum pump. Thereafter, solution is placed on the substrate, so that the surface is completely wetted. To create the film, the rotating plate rotates at high speed to spread the fluid. The solvent is either spinning of the edges or evaporates. The rotation continues until the solute has formed a film with the desired thickness, which depends on the angular speed and on the concentration of the solvent in the solution. Higher speed of the spinning and less concentration leads to thinner films.

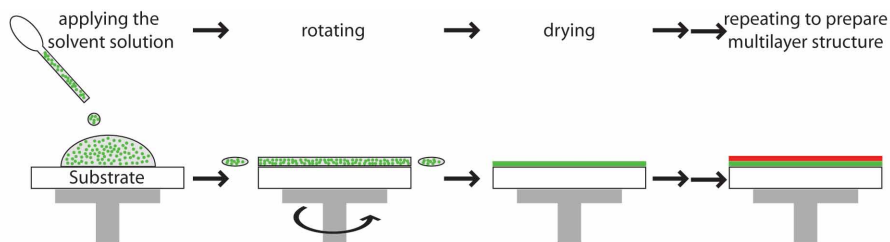


Figure 2.1: The main steps of the spin-coating process [20]

## Cellulose

Since cellulose is resistant to various solvents, a good and easy way to manufacture ultrathin cellulose films, is to use trimethylsilylcellulose (TMSC). TMSC is produced by exchanging the OH groups of the cellulose with  $Si(CH_3)_3$  groups. Because of the significant reduction of the intermolecular hydrogen bonds, this silylated cellulose derivative can be solved in a nonpolar solvent. The TMSC film is then transformed back to cellulose by vapour phase acid hydrolysis (Figure 2.2) [21].

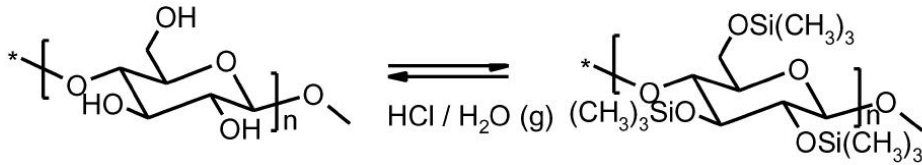


Figure 2.2: ( $\rightarrow$ ) Synthesis of TMSC out of cellulose. ( $\leftarrow$ ) Hydrolysis of TMSC to cellulose [21].

In this work a concentration of 20% TMSC is solved in the nonpolar solvent toluol ( $C_7H_8$ ). After weighing the TMSC powder with a precision balance, adding the desired amount of toluol with the micro-pipette and resting of around 6 hours, it gets mixed by a Heidolph Reax 2000 shaker until a homogenous solution is reached.

The angular speed of the spincoating is 4300rpm for around 50s, with an acceleration of 2200rpm. These parameters (concentration of the solution and angular speed) leads to a film thickness of around 50nm.

For hydrolysis a 10%-HCl solution is mixed in a desiccator. The spincoated wafers are put on a ceramic holder in the desiccator, then the vessel is closed. A waterjet pump generates a rough vacuum (minimal pressure of 2,3388kPa (steam pressure of water)), in which the wafers are exposed to the HCl-steam for around 3min. The change of the reflection colour is a good indication for the finished transformation.

To get a film thickness of  $\sim 200$ nm, which is needed to neglect any influence of the silicon substrate, this process has to be repeated 4 times. Since cellulose is not solvable in toluol, spincoating can be repeated without destroying the previous layers.

## Xylan

Xylan is spincoated on the already existing cellulose layers. For that, xylan, extracted from a beech sulfite cook [22], is solved in DMSO (Dimethylsulfoxide). Since hereby no hydrolysis is used, the desired thickness (as thick as possible, to neglect the influence of the cellulose) has to be reached in one spincoating process. That is the reason why, a limiting concentration of 50% xylan is used. Spincoating with an angular speed of 2000rpm for 40s leads to the best xylan surfaces.

## 2.2 Swelling and drying

1. After cleaning a vessel with dish soap and water, it is purged with isopropanol and acetone.

2. Next, the pot is filled with distilled water ( $\sim 1\text{cm}$  height). If ionic compounds are needed,  $0.1 \frac{\text{mol}}{\text{l}}$   $\text{CaCl}_2$  (Calciumchloride) is weighed and added to the fluid.
3. The films are carefully put inside and the vessel is closed with an aluminiumfoil. The swelling takes around 13h (Figure 2.3).
4. After swelling, the films are put into a Rapid-Köthen shelf drier. The arrangment inside the drier is illustrated in Figure 2.4. The drying lasts for 4h at  $90^\circ\text{C}$  at a pressure of  $\sim 0.1\text{bar}$ .
5. The dried samples are taken out of the drier and stored in the climate chamber for  $\sim 19\text{h}$ . In that room the conditions (temperature of  $23^\circ\text{C}$  and a relative humidity of 50%) are well defined.

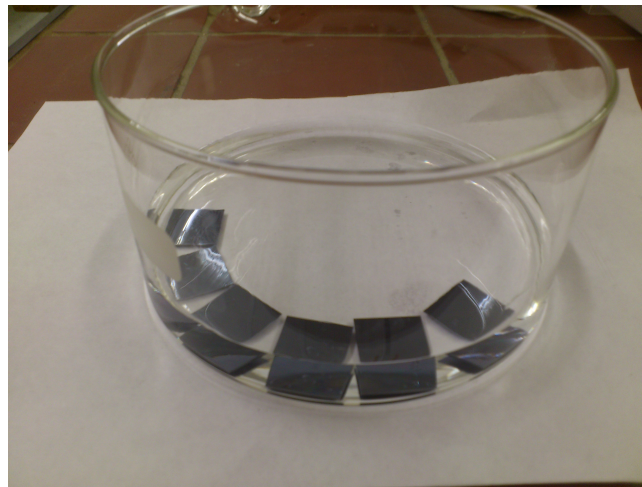


Figure 2.3: Swelling of the films inside a vessel.

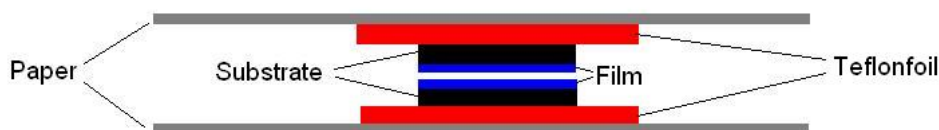


Figure 2.4: The arrangment inside the shelf drier.

## 2.3 Tensile tests

After the samples are dried and the bonds have formed, a tensile test is performed. For that, the two films get torn apart. This procedure is executed by a modified Freeman Technology FT4 Power Rheometer, which normally is used to investigate powder samples (Figure 2.5, left). It mainly consists of a lower and an upper cylinder, whereby the upper cylinder is able to move up and down due to a linear motor.

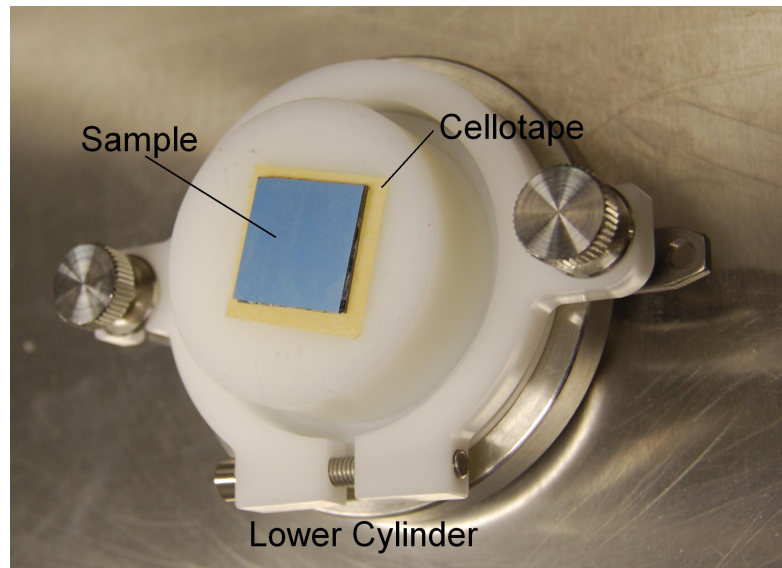


Figure 2.5: Modified power rheometer

To execute the tensile test, first a double-sided cellotape is stuck on the upper cylinder and the lower cylinder. The sample is then placed on the lower cylinder (Figure 2.5 right). For getting the best bonding between sample, cellotapes and cylinder [23], the linear motor of the apparatus moves the cylinder down until it touches the sample (point 1 in Figure 2.6). Now the force gets increased until a compression force of  $40\text{N} \pm 10\%$  is reached (point 2). After the pressure is held for 20s, the cylinder moves up, until the contact-pressure reaches the zero-line, when the actual test is starting (point 3).

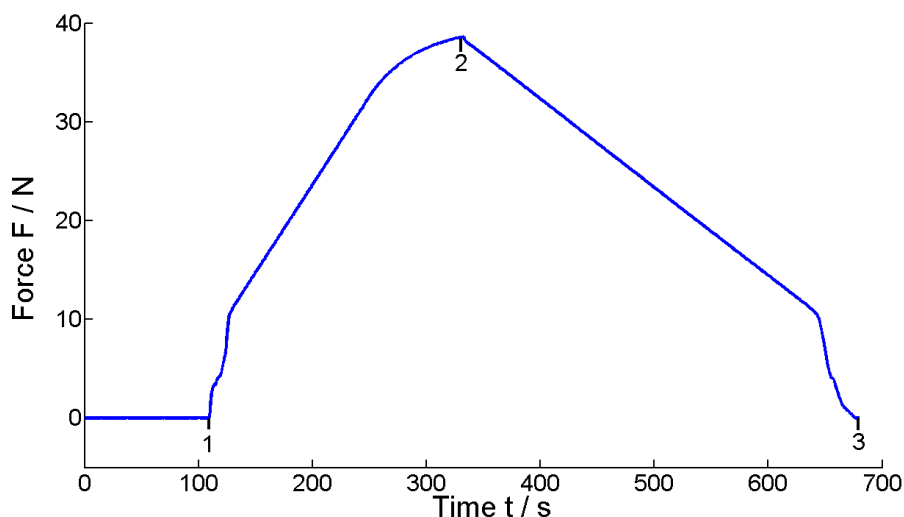


Figure 2.6: Test procedure before the actual tensile test. The force  $F$  is illustrated with respect to the time  $t$ .

### 2.3.1 Calculation of the data

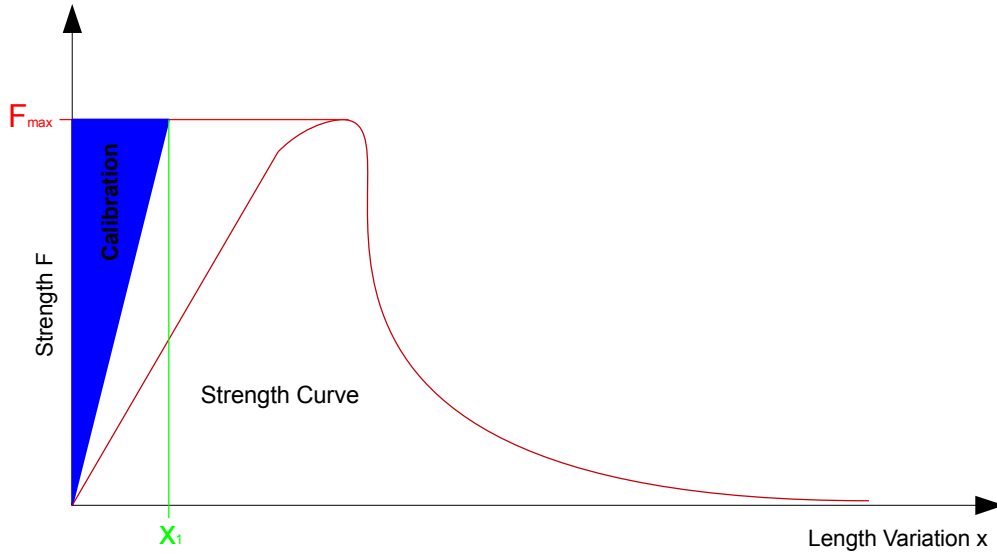


Figure 2.7: A sketch of a typical tensile-test result. The force  $F$  is plotted with respect to the length variation  $x$ . Included is the linear fit of the calibration.

The two main values for interpreting the tensile tests, is the maximum strength of the bonds  $F_{max}$  and the bonding energy per area  $E_b$ . The, for the analysis used Matlab code is illustrated in Appentix A.

$F_{max}$  is the maximum of the strength curve in Figure 2.7 and, therefore, is easy to calculate by searching the highest value of the measured data.

The energy is the integral of the force  $F$  after the length variation  $x$  (Equation 2.1), which is the area under the strength curve.

$$E = \int F \cdot dx \quad (2.1)$$

However the double sided cellotape, which is used to fix the sample to the setup, absorbs part of the incoming energy (labeled Calibration in Figure 2.7). By using equation 2.2 the true value is calculated:

$$E = E_m - E_{tape} \quad (2.2)$$

- $E_{tape}$  ... Energy adsorbed by the cellotapes
- $E_m$  ... Measured energy
- $E$  ... Bonding energy

The bonding energy per area is ( $A = 4cm^2$ ):

$$E_b = \frac{E}{A} \quad \left[ \frac{J}{m^2} \right] \quad (2.3)$$

## Calibration

Two cleaned silicon-substrates are glued together with a cyanacrylat-glue. The rough surfaces are pointing to the outside. The data obtained in the tensile tests is approximated with a linear fit:

$$F_{tape} = k \cdot x + d \quad (2.4)$$

The Energy  $E_{tape}$  is the area under this curve, with  $x_1$  being the length variation at  $F_{max}$  (Figure 2.7)

$$E_{tape} = \int_0^{x_1} F_{tape} dx \quad (2.5)$$

## Caluclation of $E_m$

Since the measured strength curve is very difficult to fit, and this fit might not even be integrable, the calculation is done with the Matlab-algorithm “trapz(F,x)”, which uses trapezoidal integration to solve the integral 2.1.

### 2.3.2 Statistical analysis

Even by producing the samples always the exact same way, the results of the tensile tests are fluctuating around the calculated mean value. For this reason, the experiments have to be repeated several times. The collected results are then investigated by the following procedure:

1. First the results are analysed to see which experiments are valid. Invalid results, e.g. bad sample preparation, are removed.
2. The mean value and the variance of  $F_{max}$  is calculated ( $\overline{F}_{max}$  and  $\sigma_F$ )
3. Since natural materials and their key values are often normal distributed, it is evident to perform a normal distribution test. For quantities of around 20-30 samples, a Q-Q-plot (quantile-quantile-plot), also called probability plot, is a very good estimator. Hereby the data is plotted with respect to a theoretical distribution (in this case the normal distribution). If the points are approximately following a straight line, it can be assumed that the results follow the specified probability distribution. It has the big advantage that different to other tests, outliers are not effecting it thus can be easily detected. Examples are illustrated in Figure 2.8 [24].

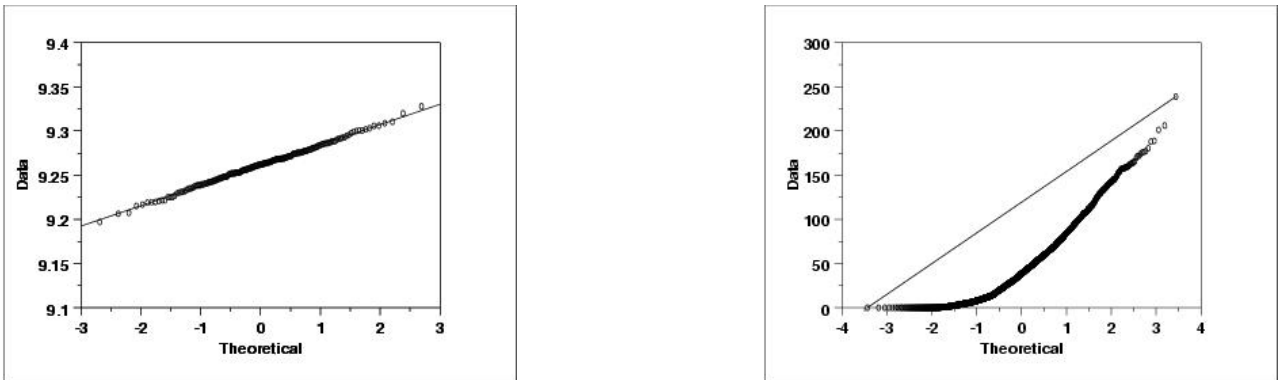


Figure 2.8: Examples for Q-Q-plots: Left for normal distributed data, right for not normal distributed data [24].

4. If the results are indeed normal distributed, an outlier test after Grubb is performed. Statistical outliers are values which are incompatible to a certain probability function [25]. If not detected, these values can strongly influence the analysis of the experiment. A detailed instruction of the Grubb test can be found in [26].
5. Out of the remaining values, the mean value and the variance of the bonding energy ( $\overline{E_b}$  and  $\sigma_E$ ) are calculated.
6. Finally, to see if the difference between the in chapter 2.4 described experiments is significant, a t-test is performed. A t-test is checking if normal distributed mean values of 2 different experiments are equal or not. A more detailed description of the t-test is illustrated in [27].

## 2.4 Task

For understanding the importance of different influences the following settings are investigated:

1. Cellulose - Cellulose, swelled in distilled water: Hereby, cellulose without any other influences is investigated. Only Van-der-Waal and hydrogen bonding is contributing to the total strength.
2. Cellulose - Cellulose, swelled in ionic water, by solving  $CaCl_2$  in distilled water. The main question is, if the ionic elements can attach to the cellulose and if coulomb bonds between the two films occur.
3. Xylan - Xylan, swelled in distilled water: In this experiment, xylan without any ionic influences is studied, to determine if and why this configuration leads to an increase of strength compared to the cellulose. Therefore, xylan is spincoated on already finished cellulose layers (Chapter 2.1).
4. Cellulose - Xylan: The goal is to determine, how well these two different molecules are bonding to each other.
5. Xylan - Xylan with stored DMSO (Dimethylsulfoxide). The solvent remains on the substrate during spincoating and also diffuses into the already existing cellulose layers. The question is, if that has an influence to the swelling behaviours of the xylan.
6. Xylan - Xylan, swelled in ionic water: What influence do cations attached to the xylan acide-groups have to the film bonding.

## 2.5 Nanoindentation

Nanoindentation is the hardness investigation of microscopic samples, like the produced films. As explained in chapter 1.4.2, swelled films experience a strong reduction in penetration hardness. By investigating the hardness of the produced films before and after swelling it might be possible to get an idea about the swelling behaviour of the specific setting.

For that a three-sided pyramid fixed on the end of the cantilever in an atomic force microscope (AFM) is pressed into the film (Figure 2.9).

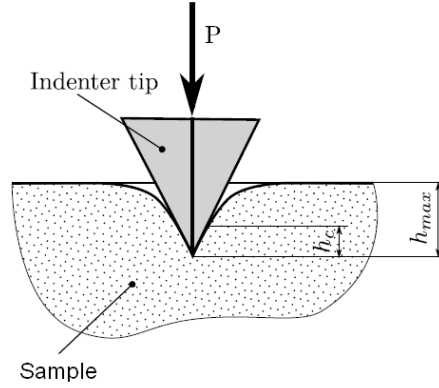


Figure 2.9: Schematic illustration of a nanoindentation experiment [28]

The experimental procedure is sketched in Figure 2.10. First the pyramid is pressed into the sample with a rate of  $10 \frac{\mu N}{s}$  until a maximum load of  $10 \mu N$  is reached. This pressure is held for 10s to allow thermal drift compensations, after which the the pressure is released with a rate of  $-10 \frac{\mu N}{s}$ . At a load of  $0.5 \mu N$  the pressure is held for 30s, to again allow thermal drift compensations.

The hardness  $H$  is calculated by equation 2.6.

$$H = \frac{P_{max}}{A_c(h_c)} \quad (2.6)$$

$P_{max}$  ... Maximum load

$A_c(h_c)$  ... Projected contact area at  $P_{max}$ , measured at 1 in Figure 2.10 right

The reduced modulus  $E_r$  is determined by:

$$E_r = \frac{\sqrt{\pi}}{2} \cdot \frac{S_e}{\sqrt{A_c(h_c)}} \quad (2.7)$$

$S_e$  ... Elastic stiffness

The elastic stiffness  $S_e$  is the slope at the beginning of the unloading part. This can be determined by the linear fit ("Fit Unld") in figure 2.10 left.

The nanoindentation measurements are executed by Christian Ganser of the Montan University of Leoben and are published in [29].

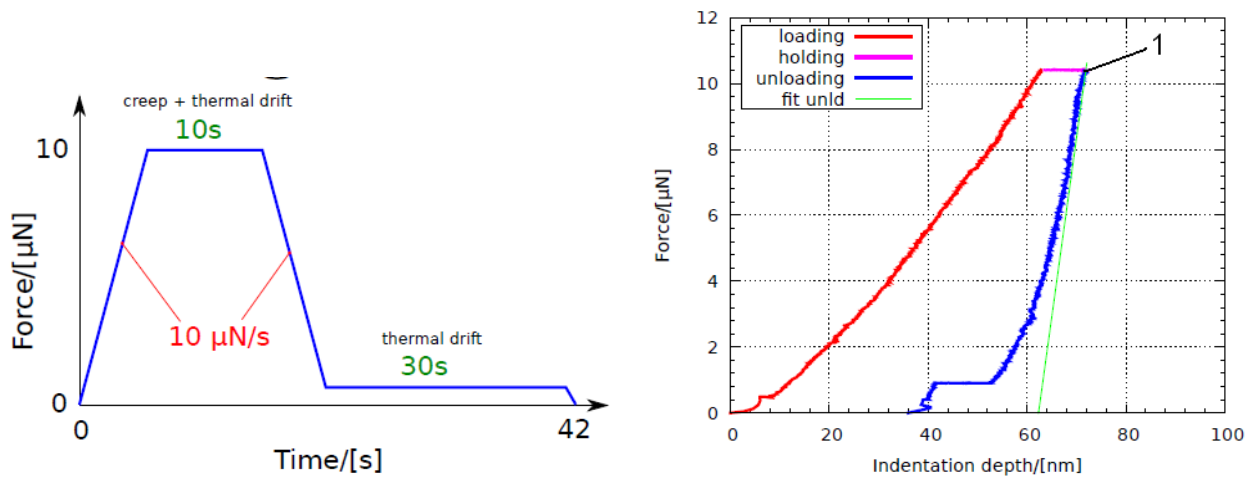


Figure 2.10: The experimental procedure of an AFM nanoindentation experiment (left) and the experimental result (right) [28].

# Chapter 3

## Measurements and results

### 3.1 Calibration

To calculate the bonding energy, it is essential to know the energy absorbed by the double sided cellotapes on both sides of the sample during the tensile test (Chapter 2.3.1). Instead of a cellulose sample two glued together silicon wafers are placed in the machine. By using a strong cyanacrylat glue it is ensured that the measured energy is identically to the energy absorbed by the cellotapes. In total 6 measurements were carried out (Figure 3.1).

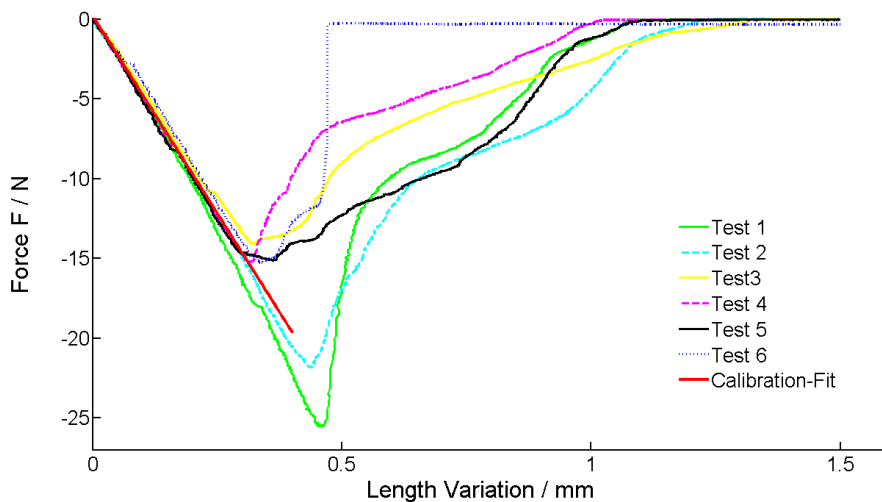


Figure 3.1: Measured data and the linear fit for the calibration of the double sided cellotape. The force  $F$  is illustrated over the length variation  $x$ .

The obtained data shows a linear increase of strength until a maximum point is reached. Hereby most of the cellotape detaches of the sample and thereby the force is decreasing. However some parts of the cellotapes are still attached to the sample and that is why the force is not decreasing to zero immediately.

Since the cellulose samples separate well before the cellotapes detach, only the linear part of the curves are of interest for this work. For this purpose every curve is approximated by the linear fit (Equation 2.4).

Table 3.1: Fit of the the strength curves in the linear range.

k ... Slope of the linear fit  
d ... Offset

Test	k / $\frac{N}{mm}$	d / N
1	-53,6758	0,3429
2	-50,0169	0,1895
3	-46,1766	0,1660
4	-49,7263	0,0242
5	-50,3908	0,0324
6	-47,5638	0,4852

Out of the fit parameters, illustrated in Table 3.1, the mean values, which are used in the following chapters, are calculated:

$$\bar{k} = (-49,6 \pm 2,6) \frac{N}{mm}$$

$$\bar{d} = (0,21 \pm 0,18) N$$

This fit is valid in a range until 13N and is pictured in Figure 3.1. The calculation of the energy absorbed by the cellotapes is illustrated in chapter 2.3.1.

## 3.2 Cellulosefilm

### 3.2.1 Infrared spectroscopy

for two reasons are the produced cellulose films investigated with reflection-absorption-infrared-spectroscopy (RAIRS):

1. To determine, if the hydrolysis does indeed completely transform the TMSC to cellulose.
2. By integrating the area under an absorption peak, an estimation of the film thickness can be obtained [14].

The advantage of RAIRS is, that compared to other popular techniques like X-ray photoelectron spectroscopy, it provides information about the organic compounds of a polymer material. The RAIRS spectra were measured by using a reflection unit with a variable angle and a polarizer from Bruker Optics. These measurements are performed under vaccum and with an incidence angle of 74°. In contrast to normal infrared spectroscopy, polarized light is used. For s-polarized light the electric field vector  $\mathbf{E}$  is perpendicular to the plane of incidence, for p-polarized light  $\mathbf{E}$  is parallel to the plane of incidence.

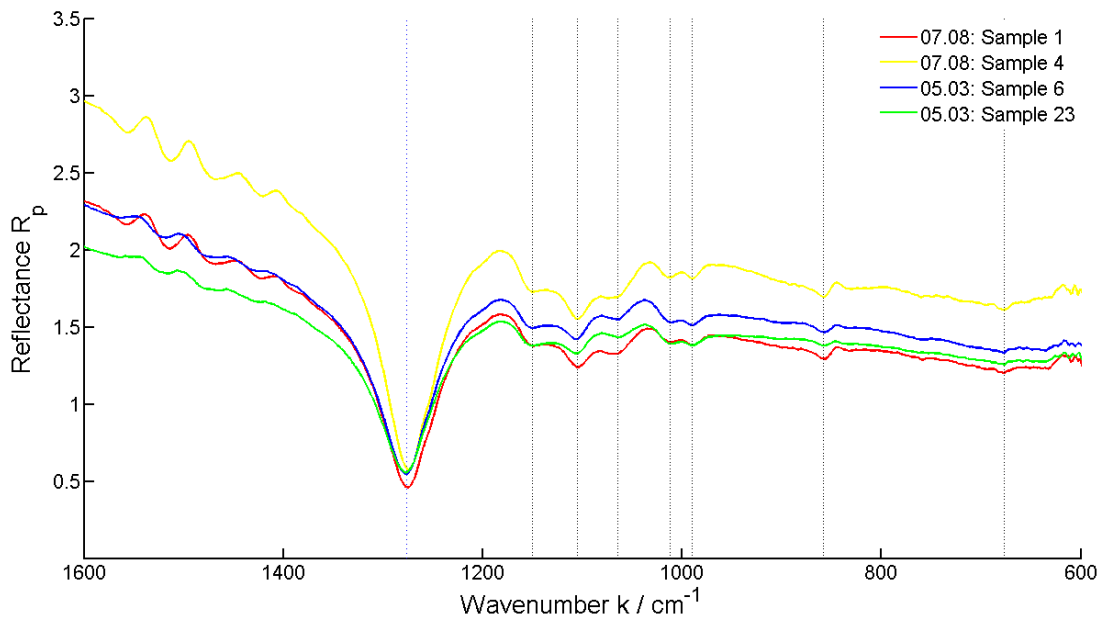
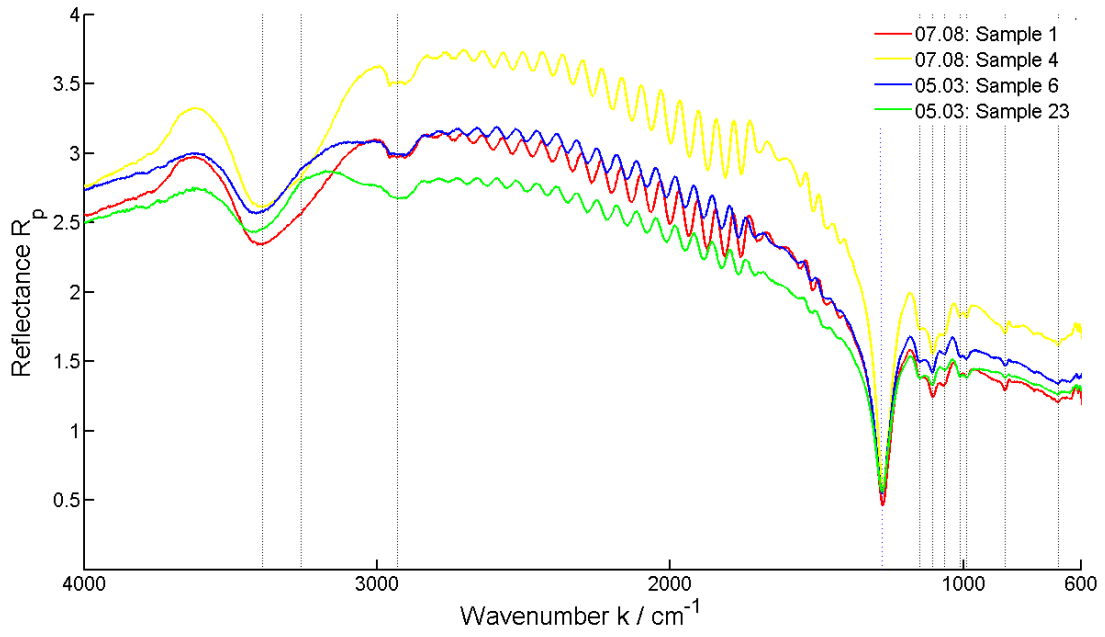


Figure 3.2: Reflection p-spectra of 4 random chosen cellulose samples. The spectra above are plotted over the whole wavenumber region, the figure below shows the results in the fingerprint region. Die dotted lines indicate the peaks at following positions (from right to left): 677, 858, 990, 1012, 1065, 1105, 1150, 1274 (blue), 2930, 3260, 3390

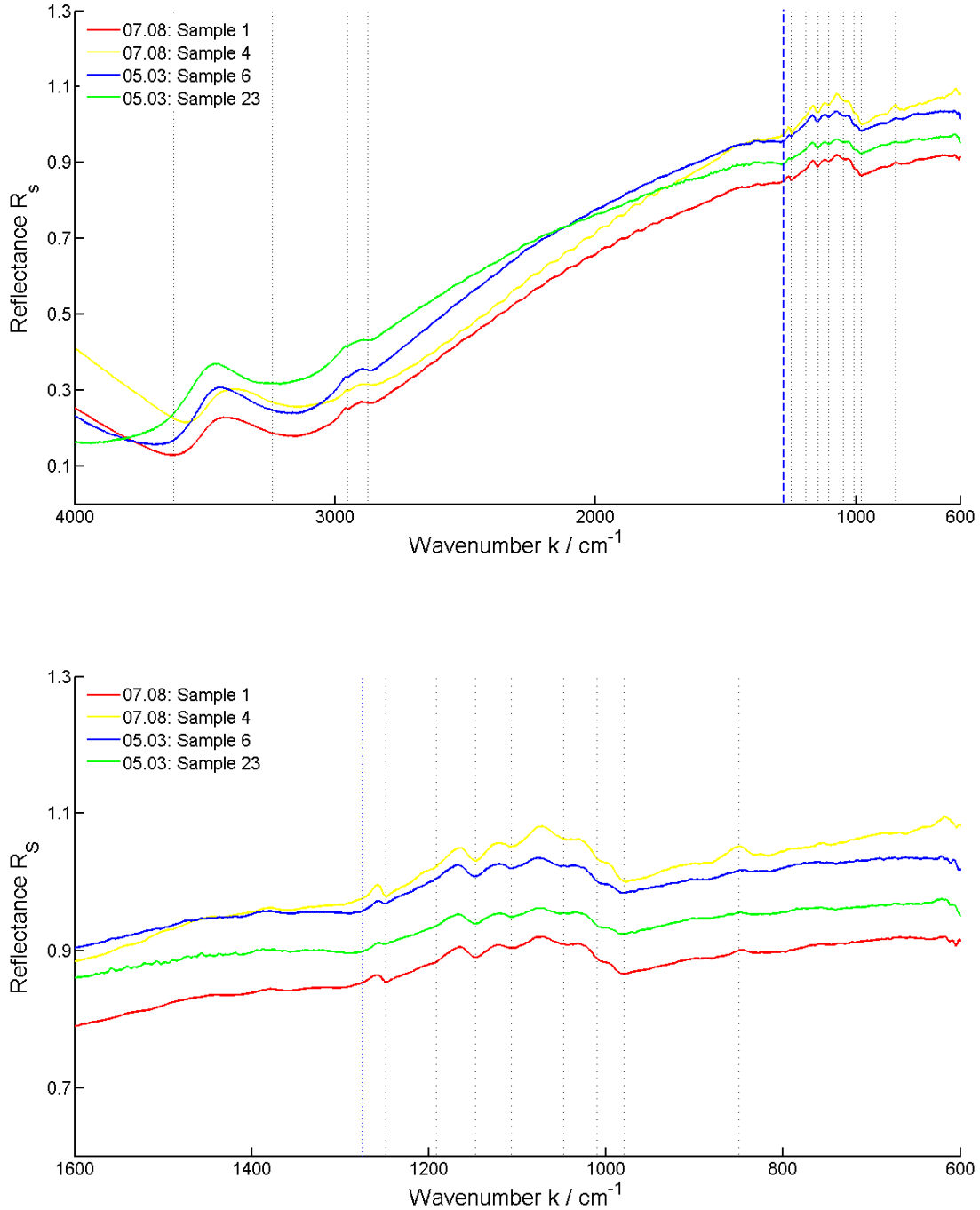


Figure 3.3: Reflection s-spectra of 4 random chosen cellulose samples. The spectra above are plotted over the whole wavenumber region, the figure below shows the results in the fingerprint region. Die dotted lines indicate the peaks at following positions (from right to left): 850, 980, 1010, 1048, 1107, 1147, 1192, 1249, 1274 (blue), 2875, 2952, 3240, 3620

The s- and p-polarized spectra of 4 random chosen samples are illustrated in Figure 3.2 and 3.3. The used reference is a cleaned silicon substrate. The absorption peaks which are due to excitation of different oscillation modes, are indicated with dotted lines and compared with literature values and values obtained for similar produced cellulose films in Table 3.2.

The dominant peak in the p-spectrum at  $1275\text{cm}^{-1}$  (marked with the blue line) is not explained by any literature data. At this wavenumber there is no absorption for s-polarized light. The reason is the so called Berremann effect. Hereby an additional oscillator is caused by the

thin films structure. This effect only causes absorption for p-polarized light. That is why all Berremann peaks only exist in the p-spectrum and can be detected by subtracting the s-spectrum from the p-spectrum. The absorption intensity depends on the film thickness, while the frequency is nearly not shifting. This can be used for measuring the thickness of the film, but is not used in this work [30].

The peaks in the fingerprint region ( $600 - 1600\text{cm}^{-1}$ ) match good with the literature and the reference data. The peaks at low frequencies ( $<900\text{cm}^{-1}$ ) are not visible or a little bit shifted, which might be due to machine inaccuracy. In the p-spectrum the peaks between  $k = 1200 - 1300\text{cm}^{-1}$  overlap with the dominant berremann-peak and, therefore, cannot be registered. However, since the s-spectrum displays them, these absorbtions definitely take place. In the wavenumber-range of  $1400 - 2600\text{cm}^{-1}$  the Fabry-Perot interference effect dominates. This effect depends on the film thickness and the refraction index of the material.

The peaks at high wavenumber fit again well to the literature and reference data. As indicated in [14], the intramolecular hydrogen bonding ( $3410 - 3469\text{cm}^{-1}$ ) is dominant compared to the intermolecular hydrogen bonding ( $3230 - 3310\text{cm}^{-1}$ ). That is why in the p-spectrum only one peak can be observed. Since the glaciation of the detectorwindow is interfering the results between  $3200 - 3350\text{cm}^{-1}$ , the position and the intensity of the peaks can vary between the different tests.

Table 3.2: Absorptionpeaks of cellulose. The measured values (Experiment) are compared to literaturevalues (Literature) and to values obtained for same produced cellulose-films at the same interferometer(Reference). Most of the literature data is abstracted from [31]. The reference data is recorded in [14].

k $cm^{-1}$	Literature	Reference		Experiment	
	Molecule / Oscillation	s $cm^{-1}$	p $cm^{-1}$	s $cm^{-1}$	p $cm^{-1}$
663	OH bending	665	670		677
893-895	Antisym. orbital stretching	895	898	850	858
900-910	CH bending; $CH_2$ stretching				
1000	CO or CC stretching	1019	998	980	990
1015	CO stretching			1010	1012
1035	CO stretching	1048	1032	1048	
1060	OH bending		1066		1065
1070	CO stretching [32]				
1110	Antisym. orbital stretching		1098	1107	1105
1162	COC antisym. bridge stretching	1153	1153	1147	1150
1205	OH bending	1199	1199	1192	
1257	$CH_2$ swingoscillation [33]		1254	1249	
1374	CH bending	1370	1370		
1426-1430	$CH_2$ bending	1432	1432		
2870-2900	CH stretching	2900	2900	2875/2952	2900-2950
3230-3310	Intermolecular O(6)H ... O(3) stretching [34]	Streching	3260	3170-3260	3250-3300
3410-3469	Intramolecular O(2)H ... O(6) stretching [34]	3385	3385	3620-3712	3390-3420

### Thickness-Estimation

According to [14], the absorption peak intensities are proportional to the cellulose film thickness. By integrating over the area of these peaks and comparing them to the data in [14], an estimation of the cellulose film thickness can be obtained. Both measurements were done with the same interferometer and settings. In figure 3.4 the linear corrected p-spectra are illustrated in the wavenumber range of  $2800-3000cm^{-1}$ . Table 1 shows the integrated area and the resulting cellulose film thickness. The resulting mean value and its standard deviation is:

$$\bar{d} = (315 \pm 75) \text{ nm} \quad (3.1)$$

Since these experiments and the reference measurements were done at completely different times and the spectra, although similar, are not equal, this value is just a coarse estimation. Nevertheless, as the comparison with the data of the atomic force microscope measurements in chapter 3.2.2 shows, it is an easy and quick way to inspect the thickness of produced cellulose films.

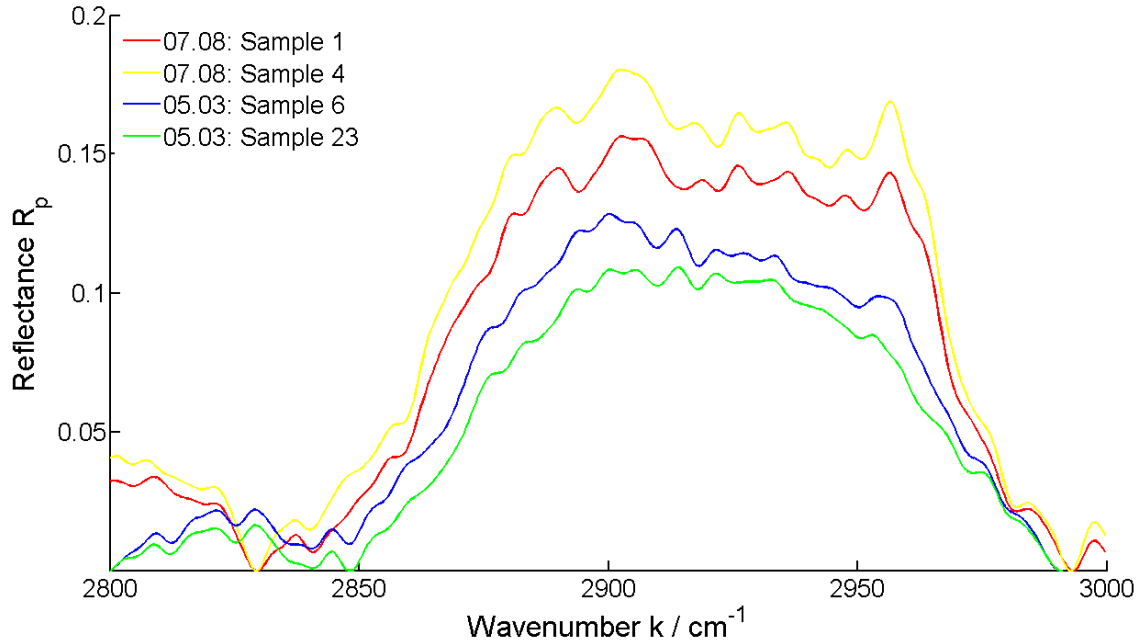


Figure 3.4: The reflection p-spectra of the 4 samples at the wavenumber range of the  $CH_2$  bending absorption.

Table 3.3: Integrated area in the range of 2800-3000  $cm^{-1}$  and the resulting film thickness.

I ... Peakintensity  
d ... Estimated thickness of the cellulose film

Sample	I / $1 \cdot cm^{-1}$	d / nm
07.08: Sample 1	16,0	350
07.08: Sample 4	18,7	400
05.03: Sample 6	12,3	280
05.03: Sample 23	10,3	230

### 3.2.2 AFM examination of the films

To check, if the thickness estimation by RAIRS is usable and to get an idea about the swelling behaviour of the films, atomic force microscopy (AFM) is used.

Therefore, parts of one cellulose film, which is not investigated by RAIRS, are scratched off the substrate and the resulting edge is scanned with the tip of the AFM. Furthermore it is even possible to determine the thickness of every spincoated layer and also the thickness of the film in the swelled state. The results are illustrated in Figure 3.5 and in Table 3.4.

Table 3.4: Thickness of the Film in the dry and the wet state, measured with an AFM.

Sample	h / nm	$\Delta h$ / nm
Dry Film (Total)	430	5
Dry Film (One Layer)	110	10
Wet Film (Total)	690	15
Wet Film (One Layer)	150	20

The thickness of the dry film is bigger than the result obtained by the RAIRS-technique, but since it was a different film, RAIRS is definitely valid for a first estimation, or for controlling the film production. Furthermore, the films are around 2 times thicker then, as in chapter 2.1 and reference [23], predicted. This circumstance however, has no influence to the performed tensile tests.

For two reason, the individual spincoated layers have roughly the same film thickness. First, the standard deviation of the mean value is small and second the mean value multiplied by 4 is in the range of the total mean value.

As anticipated, the thickness of the film increases through swelling. The ratio of the film thickness groth is 1.6, which is quite close to the predicted maximum grow ratio of  $\frac{d_{max}}{d_0}=1.7$  (Chapter 1.4). Since the swelling time was just around 30min compared to  $\sim 13h$  during the tensile test experiments, the maximum swelling ratio might have been reached by increasing this time.

These measurements were done by Harald Plank and Timothy Aschl of the Institute for Electron Microscopy of the TU Graz (FELMI) and of the Graz Centre for Electron Microscopy (ZFE Graz).

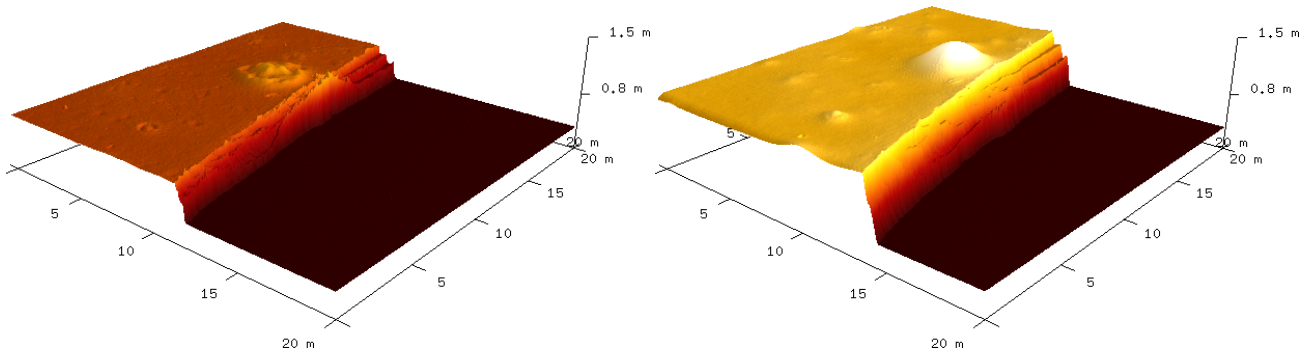


Figure 3.5: AFM images of the film before (left) and after swelling (right). The axes are scaled in  $\mu\text{m}$ .

### 3.3 Cellulose swelled in distilled water

Table 3.5 shows the tensile test results for cellulose swelled in distilled water. In 6 series, 43 tests were performed. The tests, marked by  $N_{number}$ , are invalid. The reasons for the invalidity are explained below.

Table 3.5: Tensile test results for cellulose samples swelled in distilled water.

- 1 ... Series invalid
- 2 ... Series invalid
- 3 ... Cellulose film ripped of the substrate → Test invalid
- 4 ... Sample is ripped apart too early → Test invalid
- 5 ... Cellotape failed → Test invalid

1.Series	2.Series <sup>1</sup>	3.Series	4.Series <sup>2</sup>	5.Series	6.Series
$F_{max} / \text{N}$	$F_{max} / \text{N}$	$F_{max} / \text{N}$	$F_{max} / \text{N}$	$F_{max} / \text{N}$	$F_{max} / \text{N}$
-2,0958	-0,2712	-1,5378	-0,0339	-1,5138	-1,8862
-2,0958	-0,0065	-0,7728	-0,0064	-2,3696	-2,9262 <sup>3</sup>
-9,7806 <sup>3</sup>	-0,6183	-2,1502 <sup>3</sup>	-0,9326	-1,1848	-1,8798
-2,5218	-0,6216	-1,5772	-0,0068	-4,2133 <sup>3</sup>	-4,1858 <sup>3</sup>
-2,2310	-1,0003	-1,1146	-0,0068	-1,6384	-2,0496
-0,0061 <sup>4</sup>	-0,6440	-3,0287 <sup>3</sup>	-0,2951	-2,4955	-1,3970
				-1,9955	-4,3565
				-2,6222	-0,6007 <sup>5</sup>
				-1,5949	-1,0475 <sup>3</sup>
				-2,4362	

### 3.3.1 Reasons for experimental non-validation of tensile tests

1. Since the cellulose films are only  $\sim 400\text{nm}$  thick (chapter 3.2) the swelled films are drying quickly when put out of the water on the shelfdrier. Since the temperature of the drier is  $90^\circ\text{C}$ , the samples are dry after 10-20s. In the test series marked with <sup>1</sup>, the time to put the second film on the top of the first film was longer then 20s. The main issue was to get the films out of the water. So the lower films were already nearly dried before the sample was connected. That is why the established contact surface between the two films and, therefore, the bonding strength is significant lower.
2. In the 4<sup>th</sup> test series (marked by <sup>2</sup>) the films were connected under water, to neglect the influence of the different swelling conditions. This leads however to results well below the mean value and, therefore, this test series is invalid.
3. In the tests marked with <sup>3</sup>, one cellulose film detached of the silicon surface during the tensile test (Figure 3.6). In a) the films are still connected. In b) the films usually would have already been unbonded. Hereby however, a small part stays connected and instead one film starts to detach of the silicon-substrate. In this area the energy is not used for ripping the films apart, but for peeling the film of the substrate. In c) detaching continues, while the films stay connected. Although the films are mostly disconnected, energy still flows into the system. In d) the two sides finally disconnect, and no energy is detected anymore. A microscopic image of a sample is displayed in Figure 3.7. Since most of the detected energy and force is not used for unbonding the films, but for detaching a film of the surface, these tests are invalid.



Figure 3.6: Illustration of a detaching process during a tensile test. a) Connected films. b) Sample gets stretched. One film starts to go adrift. c) The detaching process continues, while the films themselves are still connected. d) Films disconnect.

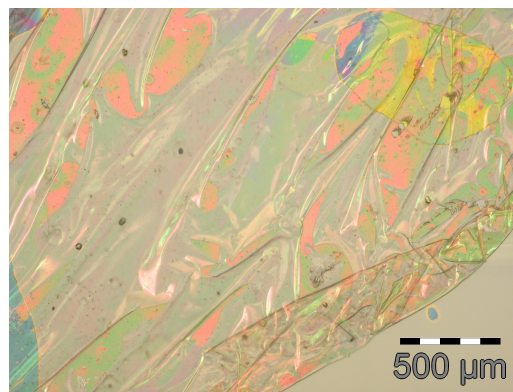


Figure 3.7: Microscopic image of a detached film.

4. In the tests marked with <sup>4</sup> the sample gets ripped apart in the pressure period (described in chapter 2.3). This event is marked by Unbonding in figure 3.8. Hereby the force performs a sudden jump before the actual tensile test, which leads to the unbonding of the sample. Since the cylinder is still pressing on the sample, this is a very unsuspected behaviour. Possible reason are external excited vibrations or a sudden force release of the springs, which generate the force inside the upper-cylinder. That is why these tests are invalid.

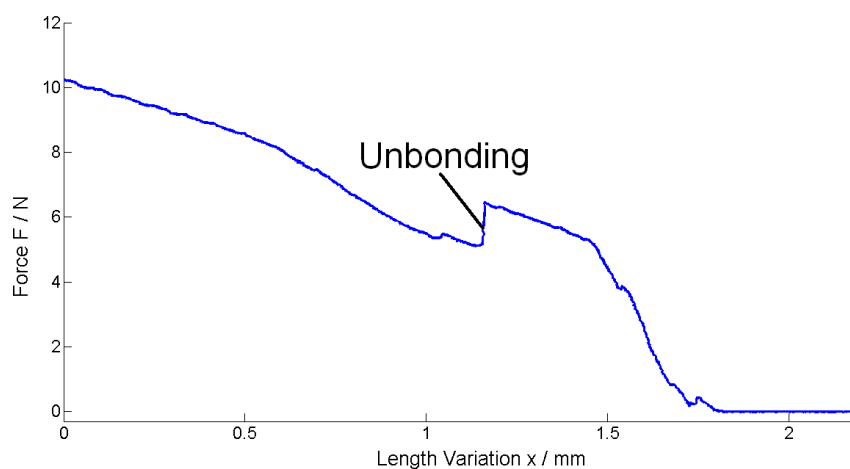


Figure 3.8: A tensile test example for an unbonding in the pressure period. The force  $F$  (N) versus the length variation  $x$  (mm) is illustrated.

5. In the with <sup>5</sup> marked test the cellotape was not placed properly on the cylinder. Due to that, the sample was not properly fixed (Figure 3.9). Since that occurred only once, no further investigations are necessary.

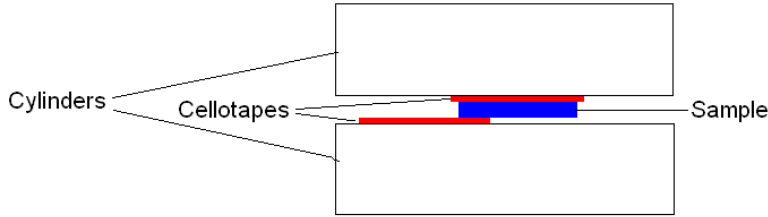


Figure 3.9: Illustration of the invalid test marked with <sup>5</sup>.

### 3.3.2 Calculation of the data

The data is calculated like in chapter 2.3.1 described:

1. The mean value and the variance of  $F_{max}$  is calculated out of the remaining values of Table 3.5:

$$\bar{F}_{max} = (-1.97 \pm 0.73) N$$

$$\sigma_F = 0.53 N^2$$

2. A Q-Q plot of the remaining results is displayed in Figure 3.10. The data is approximately following a straight line indicating normal distributed data. Only one data point (marked with a red circle) is far afield. This leads to the assumption that this point is an outlier, which is proven by an outlier test after Grubbs.

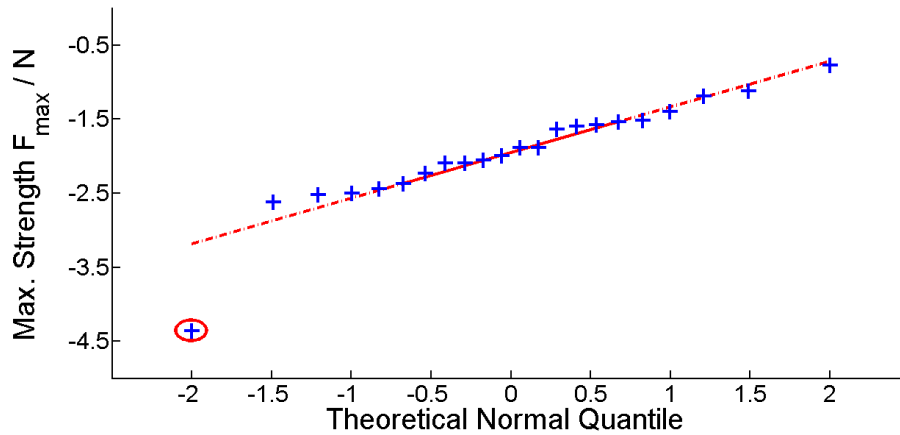


Figure 3.10: A Q-Q plot of the cellulose-cellulose results. The maximum strength  $F_{max}$  (blue crosses) is plotted with respect to the normal distribution. The red line represents perfect normal distributed data.

3. The outlier is removed, leaving the remaining data points illustrated in Table 3.6 and Figure 3.11. Included in the table is the calculated bonding energy E.

The samples are behaving alike during the testing. First the force is increasing linearly. The steepness of the curve in this area (elastic area) is proportional to the elastic modulus. Since the gradient of this increase is similar to the calibration curve, the elastic modulus for the films

and, therefore, for the cellulose is big. This indicates that the films are completely dry, since according to [19] and chapter 1.4.2, the elastic modulus is way bigger in the dry state compared to the wet state. The linear force increase continues until the maximum strength  $F_{max}$  is reached, where it strongly decreases. Just some samples, especially sample 3 and 10 show different behaviour. Their curves seem to consists of two superimposed functions. Another possible reason is that some kind of mechanical interlocking occurred and, therefore the additional peak can be attributed to this bond. Another possibility is that the films were not completely dry. This additional peak is also one reason for the big standard deviation of the bonding energy.

Table 3.6: Valid tensile tests results for cellulose films swelled in distilled water.

Nr.	$F_{max}$ / N	E / mJ
1	-2,0958	-0,2050
2	-2,0958	-0,0296
3	-2,5218	-0,7883
4	-2,2310	-0,0763
5	-1,5378	-0,0661
6	-0,7728	-0,0757
7	-1,5772	-0,1800
8	-1,1146	-0,0756
9	-1,5138	-0,2021
10	-2,3696	-0,2833
11	-1,1848	-0,1688
12	-1,6384	-0,1660
13	-2,4955	-0,1851
14	-1,9955	-0,0390
15	-2,6222	-0,1384
16	-1,5949	-0,0766
17	-2,4362	-0,1083
18	-1,8862	-0,1728
19	-1,8798	-0,2059
20	-2,0496	-0,1056
21	-1,3970	-0,0397

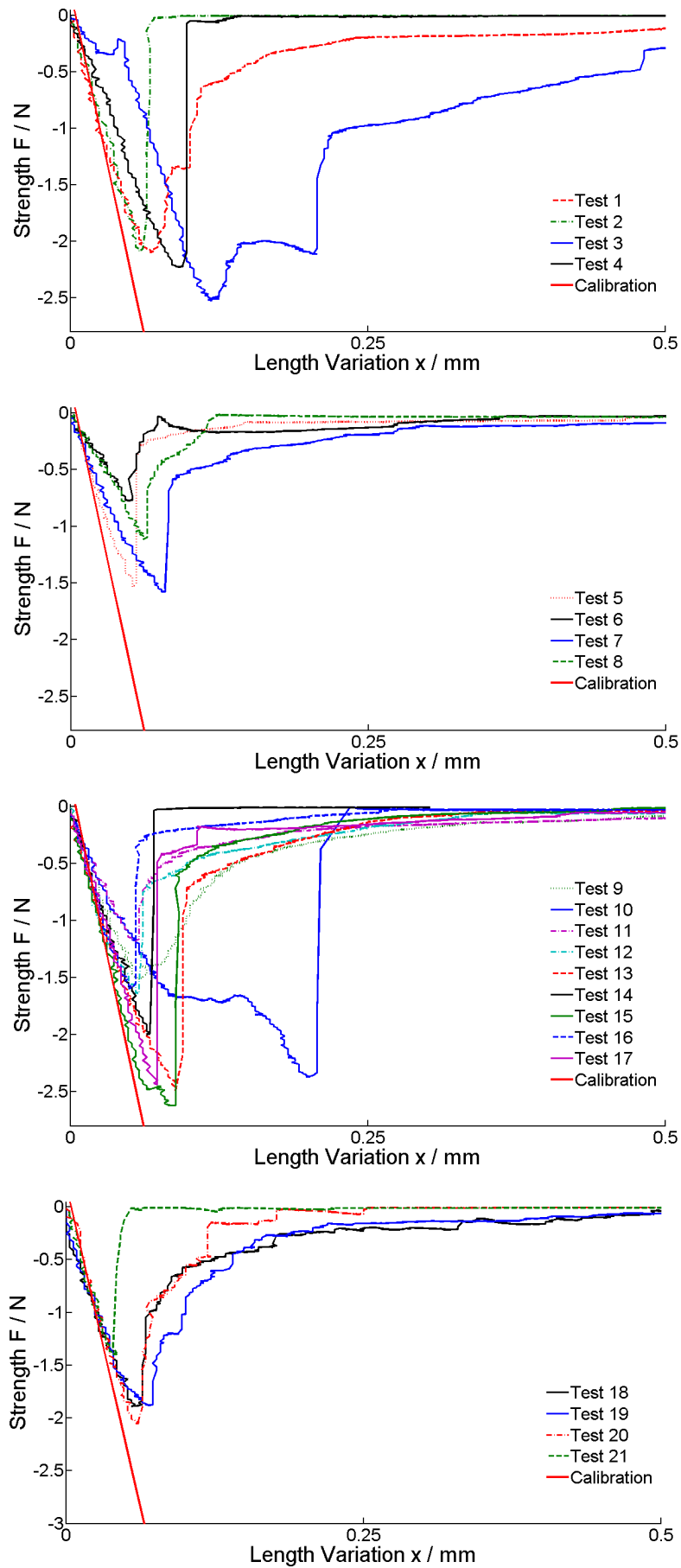


Figure 3.11: Valid tensile tests of cellulose films swelled in distilled water. The strength of the bonds  $F$  (N) is plotted in respect to the length variation  $x$  (mm). From the top to the bottom: Test series 1, test series 3, test series 5 and test series 6.

The new mean value and the standard deviation of the maximum strength  $F_{max}$  and the bonding energy  $E$  is:

$$\bar{F}_{max} = (-1,86 \pm 0,51) N$$

$$\bar{E} = (0,16 \pm 0,16) mJ$$

This value is independent of the sample area. By using equation 2.3 a comparable value is obtained:

$$\bar{E}_b = (4,0 \pm 4,0) \cdot 10^{-22} \frac{kJ}{nm^2}$$

This result is in the range of the, by [16] predicted Van-der-Waals and hydrogen bonding energies for cellulose (chapter 1.4). Although several issues, like

- big calculated uncertainty,
- films are amorphous, instead of the in the reference used crystalline structure ,
- the surfaces are not perfectly flat, which leads to not complete molecular contact,
- and the energy absorbed by the film bulk is not taken into account,

exist, the fact that both values are in the same order of magnitude, leads to the assumption that this model system provides good quantitative results.

### 3.3.3 Nanoindentation

A cellulose film is investigated right before swelling (hereafter referred to as: Dry) and right after swelling (hereafter referred to as: Wet) with the nanoindentation technique. The wet film is always kept in the completely swelled state, by a steady supply of water with the help of a pipette.

The results are illustrated in Table 3.7 and Figure 3.12:

Table 3.7: Results of the nanointentation test

H ... Hardness  
 $E_r$  ... Reduced modulus

Sample	H / MPa	$\Delta H$ / MPa	$E_r$ / GPa	$\Delta E_r$ / GPa
Cellulose (dry)	190	24	6,3	1,0
Cellulose (wet)	6,0	0,3	0,056	0,002

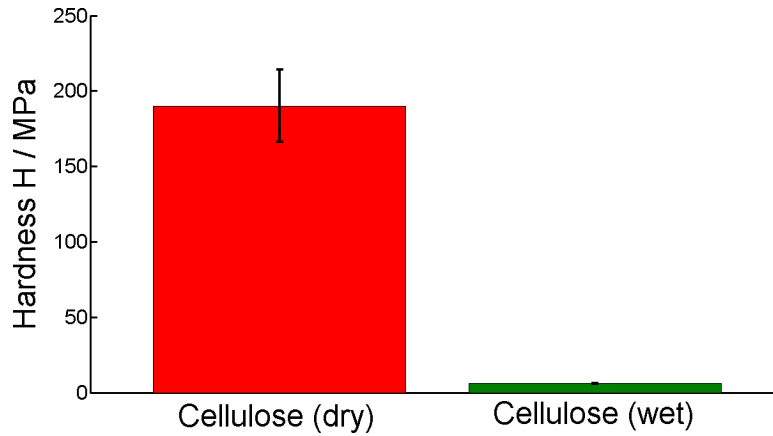


Figure 3.12: Comparison of the hardness of cellulose before (left) and after (right) swelling.

The water-molecule  $H_2O$  is breaking up the hydrogen-bonds of the cellulose (Chapter 1.4.2). This results in an enormous reduction in both hardness and reduced modulus.

During fibre-fibre and film bonding, the two wet and therefore, soft surfaces get pressed together due to the capillary forces [19]. Because of the reduced hardness, plastical deformation happens and a large contact area is formed. Since the amount of Van-der-Waals and hydrogen bonds are proportional to the contact area, the swelling behaviour of the material is crucial for the bonding strength of the films and the fibres.

That is why two dry films or fibres pressed together form no bonds, since the two surface are not in molecular contact.

### 3.3.4 Roughness-Investigation

To get an idea of the actual contact area, the roughness of two cellulose films before and after the tensile test are investigated by an atomic force microscope (AFM). For the analysis three parameters are of interest:

- $\sigma$  ... Root mean square (RMS) roughness: The standard deviation of the height values
- $\xi$  ... Lateral correlation length: An indicator for the horizontal roughness
- $\alpha$  ... Hurst parameter: An indicator for how jagged a surface is. It is between 0.5 and 1, with 0.5 being the most jagged and 1 being the least jagged

The results of these measurements are illustrated in Table 3.8:

Table 3.8: AFM investigation of two films before and after the tensile test.

		$\sigma$ /nm	$\xi$ /nm	$\alpha$
<b>Before</b>	Film 1	$31.2 \pm 5.5$	$1130 \pm 200$	$0.90 \pm 0.05$
	Film 2	$31.3 \pm 4.2$	$1130 \pm 60$	$0.90 \pm 0.05$
<b>After</b>	Film 1	$14.5 \pm 2.2$	$920 \pm 250$	$0.70 \pm 0.05$
	Film 2	$12.4 \pm 1.4$	$720 \pm 100$	$0.70 \pm 0.05$

Baesd on the data in Table 3.8 it is clear that the surfaces were in intensive molecular contact with each other. The RMS roughness is reduced to more than half and also the lateral correlation length seems to have declined, although hereby at least for Film 1 in Table 3.8 it is not significant. Maybe even more importantly also the jaggedness has declined, which is a good

indicator for flattening of the surfaces. Furthermore, both films possess deep holes after the tensile test with only a few, small hills compensating them (Figure 3.13). The cause of this effect is not completely understood yet. It might be due to small air bubbles, which evaporated during the drying process, or because of plastic deformation during the tensile test.

Because of these possible deformations during the tensile test it is also impossible to calculate the actual area in molecular contact.

These measurements were performed by Christian Ganser of the Institute of Physics at the Montan University Leoben.

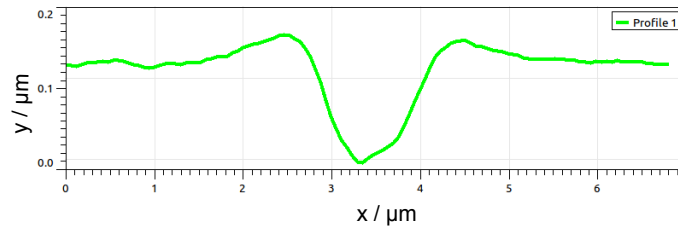


Figure 3.13: Profile across a hole in a film after the tensile test measured with an AFM.

### 3.4 Cellulose swelled in ionic water

The tensile test results for cellulose films swelled in ionic water are imaged in Table 3.9. The results marked with *Number* are invalid. The reasons for the invalidity of <sup>1</sup> and <sup>2</sup> are explained in chapter 3.3.1.

Table 3.9: Tensile test results for cellulose swelled in water containing  $CaCl_2$ .

- 1 ... Sample is ripped apart too early → Test invalid
- 2 ... Cellulose film ripped off the substrate → Test invalid
- 3 ... Crossing of the zero newton line → Test invalid

1.Series	2.Series	3.Series
$F_{max} / N$	$F_{max} / N$	$F_{max} / N$
-0,1997 <sup>1</sup>	-0,6602	-1,3331
-0,0248 <sup>1</sup>	-0,4601	-1,7505
-0,8727	-1,9171 <sup>2</sup>	-1,0822
-0,0288 <sup>1</sup>	-0,8239	-1,6856
-1,4230	-3,8483 <sup>2</sup>	-1,7232
-0,2533 <sup>3</sup>	-2,3687 <sup>2</sup>	-2,4490 <sup>2</sup>
-0,9321	-1,2520	-2,7237 <sup>2</sup>
-0,8278	-3,4183	-0,0706 <sup>1</sup>
-0,5639	-1,5105	-1,7339 <sup>2</sup>
-0,0077 <sup>1</sup>	-4,1691	-0,7310

In the tensile test marked with <sup>3</sup>, the strength curve passes the zero newton line during the experiment (Figure 3.14). That means the sample is actually pushing apart, instead of bonding

together. The reason might be a sudden force release by the springs in the upper cylinder. Since it happened just once, no further investigations are carried out.

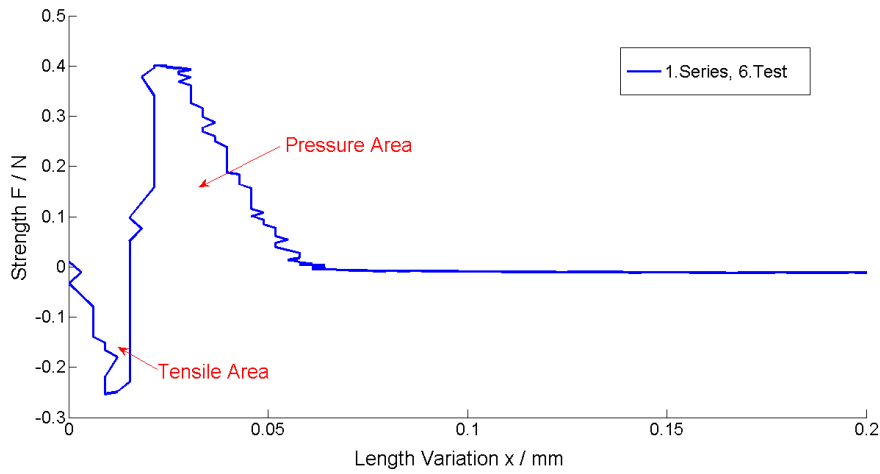


Figure 3.14: An example of the strength crossing the zero newton line into the pressure area. The force  $F$  (N) is illustrated versus the length variation  $x$  (mm).

### 3.4.1 Calculation of the data

As for cellulose swelled in distilled water (Chapter 3.3.2), a Q-Q plot is used to evaluate if the results for the maximum strength  $F_{max}$  are normal distributed (Figure 3.15). The data points, except of two (marked by red circles in the figure), are approximately following the red line representing perfect normal distributed data. To guarantee that these two results are indeed outliers, a Grubb test is used. Then they are removed from the results.

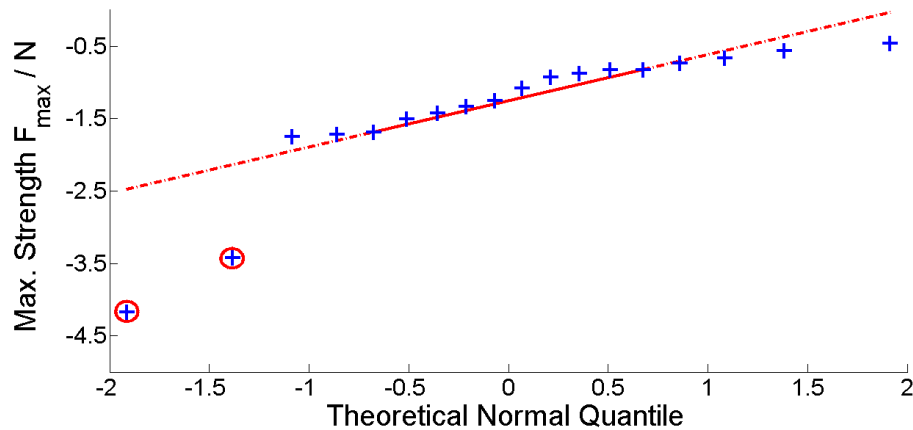


Figure 3.15: A Q-Q plot of the in ionic water swelled cellulose samples. The maximum strength  $F_{max}$  (blue crosses) is plotted with respect to the normal distribution. The red line represents perfect normal distributed data. The incircled data points indicate possible outliers.

The remaining results, including the calculated bonding energy  $E$ , are illustrated in Table 3.10 and in Figure 3.16. The tensile tests have similar behaviour as for cellulose swelled in distilled water 3.3. The area under the strength curves of the first test series (topmost figure) is smaller. The calculated bonding energies on the other hand are quite high, which is due to long ranging tales. Furthermore, the linear increase at the beginning is varying for the different tests series. This is mainly due to the inhomogeneity of the energy absorbed in the cellotapes. These two

facts are the main reasons for the quite high standard deviation of the bonding energy. Out of this results the mean values and the standard deviations of the maximum strength  $F_{max}$  and the bonding energy  $E$  are calculated:

$$\bar{F}_{max} = (-1, 10 \pm 0, 43) N$$

$$\bar{E} = (-0, 18 \pm 0, 09) mJ$$

Respectively, the bonding energy per area  $E_b$  :

$$\bar{E}_b = (4, 4 \pm 2, 2) \cdot 10^{-22} \frac{kJ}{nm^2}$$

Table 3.10: Valid tensile test results for cellulose swelled in water containing  $CaCl_2$ .

Nr	$F_{max}$ / N	E / mJ
1	-0,8727	-0,0493
2	-1,4230	-0,1739
3	-0,9321	-0,3171
4	-0,8278	-0,2349
5	-0,5639	-0,1250
6	-0,6602	-0,1797
7	-0,4601	-0,0152
8	-0,8239	-0,0749
9	-1,2520	-0,1949
10	-1,5105	-0,2277
11	-1,3331	-0,2298
12	-1,7505	-0,2327
13	-1,0822	-0,3079
14	-1,6856	-0,2066
15	-1,7232	-0,1890
16	-0,7310	-0,0521

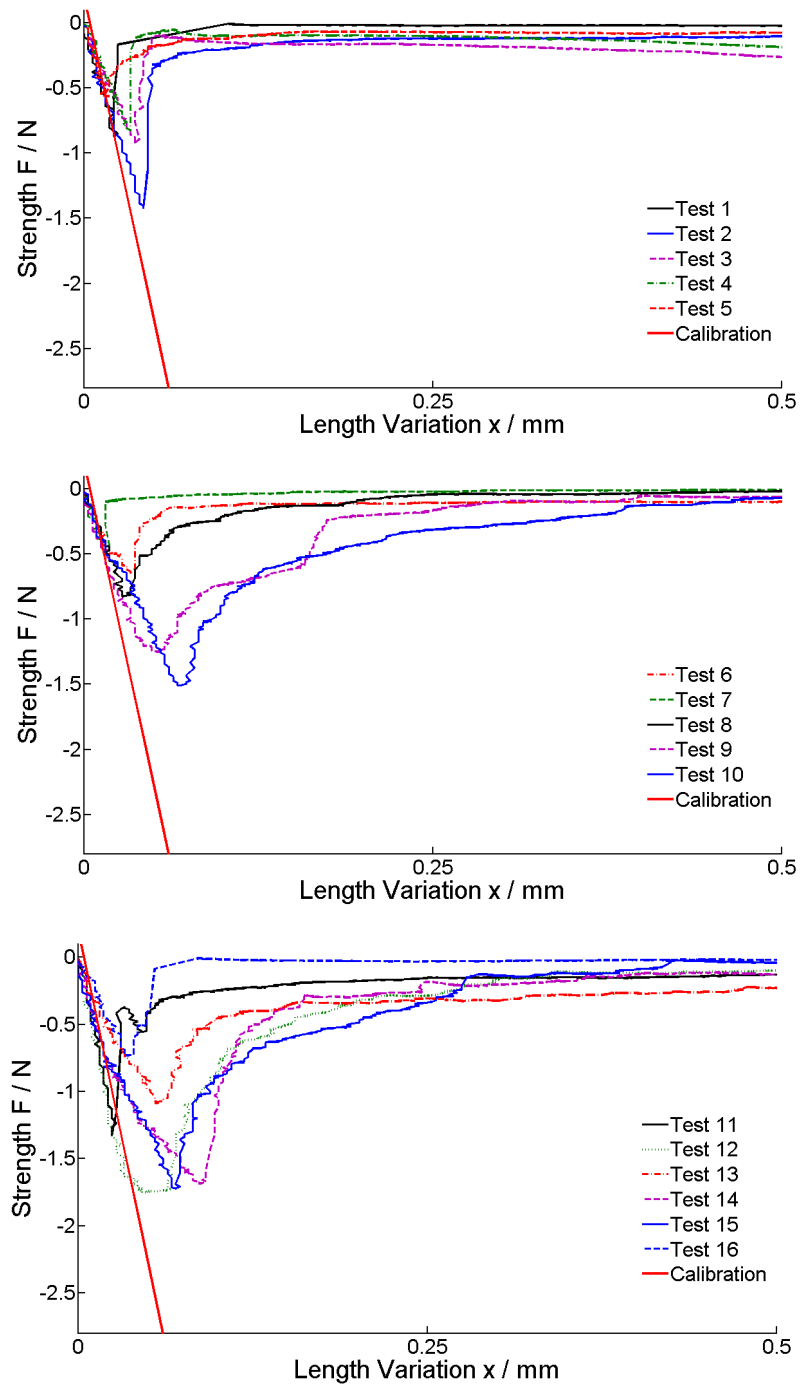


Figure 3.16: Valid tensile tests of the in ionic water swelled cellulose samples. The strength of the bonds  $F$  (N) is plotted in respect to the length variation  $x$  (mm). From the top to the bottom: Test series 1, test series 2 and test series 3.

### 3.4.2 Comparison to cellulose swelled in distilled water

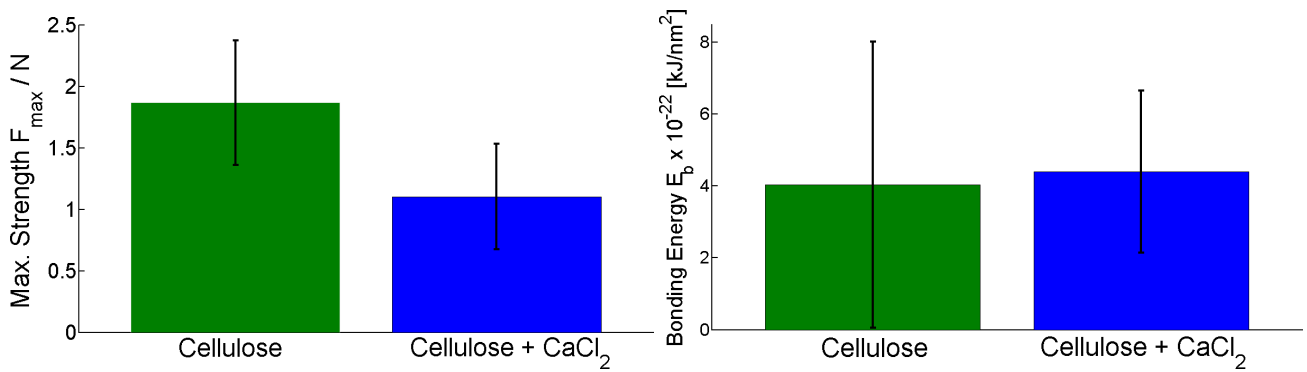


Figure 3.17: Comparison of cellulose swelled in distilled with cellulose swelled in ionic water. On the left the maximum strength  $\bar{F}_{max}$  (N). On the right the bonding energy  $\bar{E}_b$  ( $\frac{kJ}{nm^2}$ ).

In figure 3.17 cellulose swelled in distilled water is compared to cellulose swelled in ionic water. The bonding energies (right image) do not reveal any significant change. The main problem is the big standard deviations. The bonding strength (left image), on the other hand, shows a complete different behaviour. A performed t-test displays a significant strength reduction due added salt with a significant level of  $\alpha = 0.01\%$ . Used is a t-test for comparing normal distributed mean values. This reduction is visible to the naked eye by comparing Figure 3.16 with Figure 3.11.

It seems that, since cellulose molecules do not possess any strong polar endings, the cations or anions are not attaching to them. Therefore, no Coulomb interactions occur and that is why no increase in strength could be measured. Furthermore microscope images of the films after the performed tensile tests show deposited salt on the surface of the films (Figure 3.18).

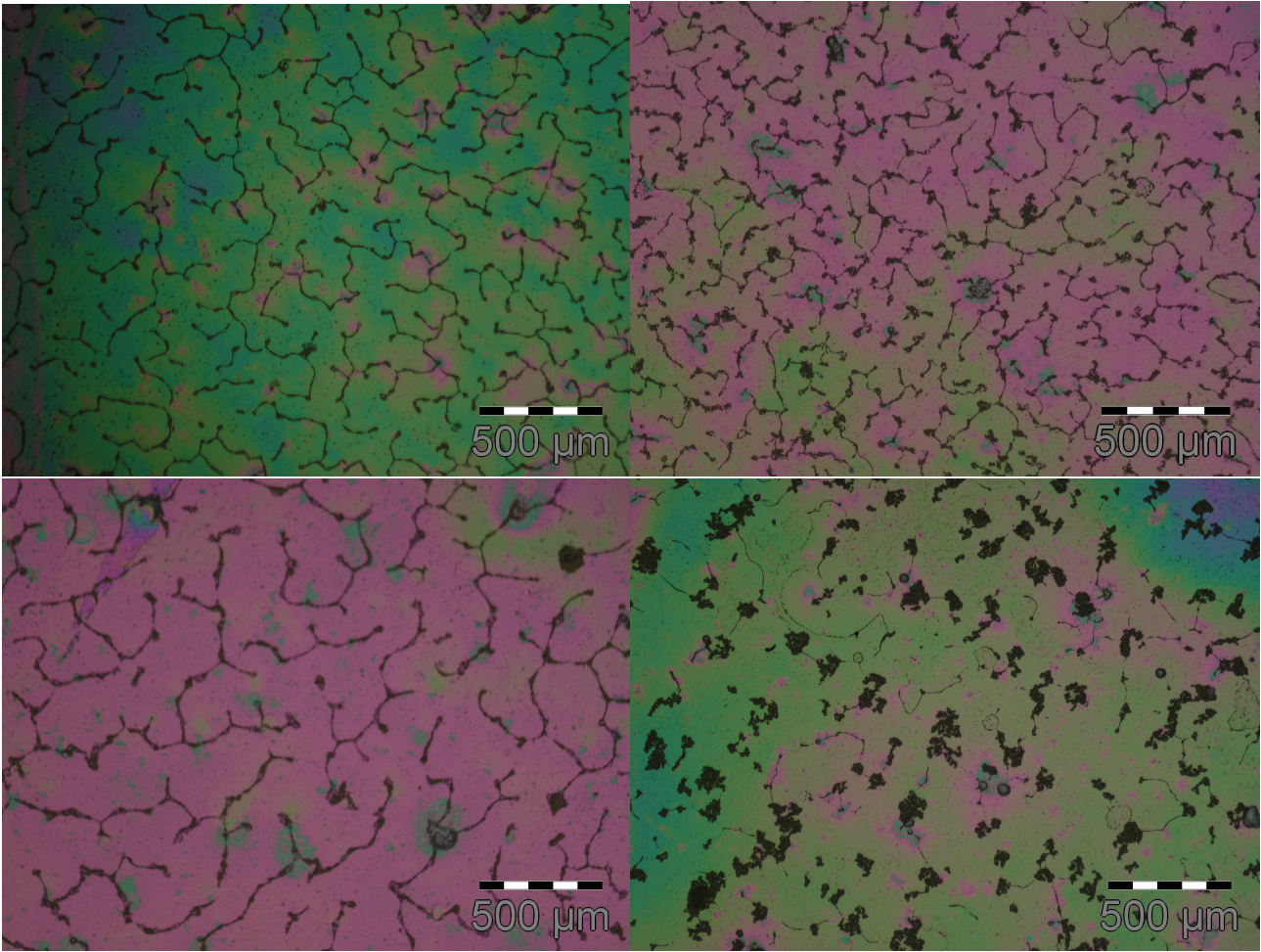


Figure 3.18: Four different microscope images of different cellulose films swelled in ionic water after the tensile test. The green and yellow background is due to the cellulose, the black lines in front are salt.

These depositions of salt are one of the reasons for the decrease of maximum strength. The salt on the surface is pushing the two bonded films apart and, therefore, decreasing the bonding area. This leads to less Van-der-Waals and hydrogen bonds (Figure 3.19).

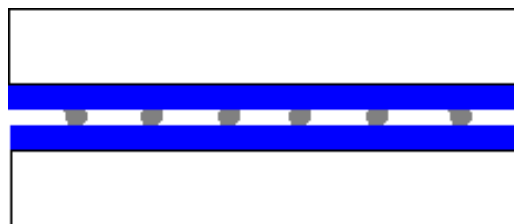


Figure 3.19: Illustration of the gap between the films due to the deposition of salt.

### Nanoindentation

The hardness and the reduced modulus  $E_r$  for a film after swelling in ionic ( $CaCl_2$ ) water are:

$$H = (7.7 \pm 0.5) \text{ MPa}$$

$$E_r = (0.063 \pm 0.003) \text{ GPa}$$

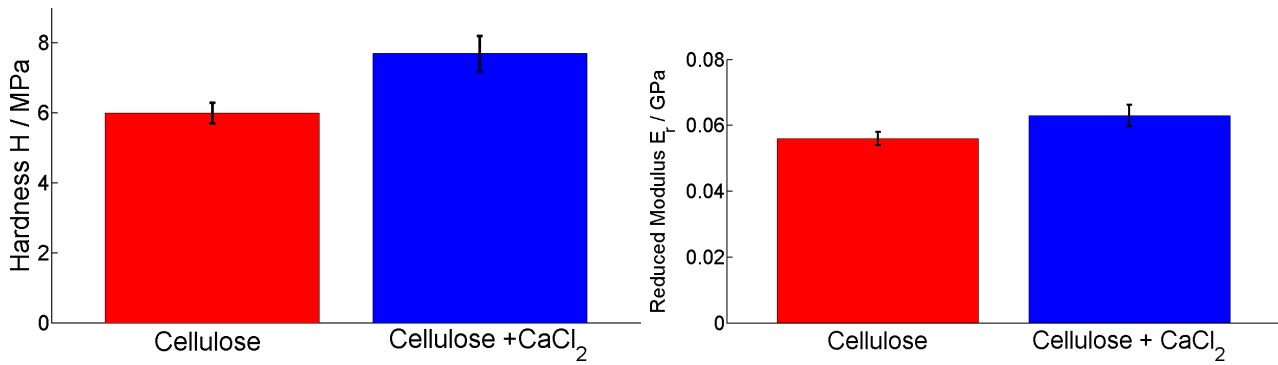


Figure 3.20: Comparison of the hardness  $H$  (left) and the reduced modulus  $E_r$  (right) of a cellulose films swelled in distilled water and in ionic water.

Figure 3.20 compares these results with the results obtained for the cellulose film swelled in distilled water (Chapter 3.3). The ions in water lead to a significant increase in hardness and reduced modulus. Therefore, the plastic deformation of films swelled in ionic water are not as strong as for films swelled in distilled water and the molecular contact area or interaction surface is smaller. For that reason less Van-der-Waals and hydrogen bonds are formed, which results in lower total strength.

During the swelling process not only water, but also  $\text{Ca}^{2+}$  and  $\text{Cl}^-$  are diffusing into the film. Water molecules are tied to these charged particles and so are not able to move free anymore (Figure 3.21). It is not very likely that these tied up molecules are breaking up hydrogen bonds. As the figure indicates the number of free water molecules in the films is reduced, which leads to less broken up hydrogen bonds during swelling and for this reason the hardness is increasing.

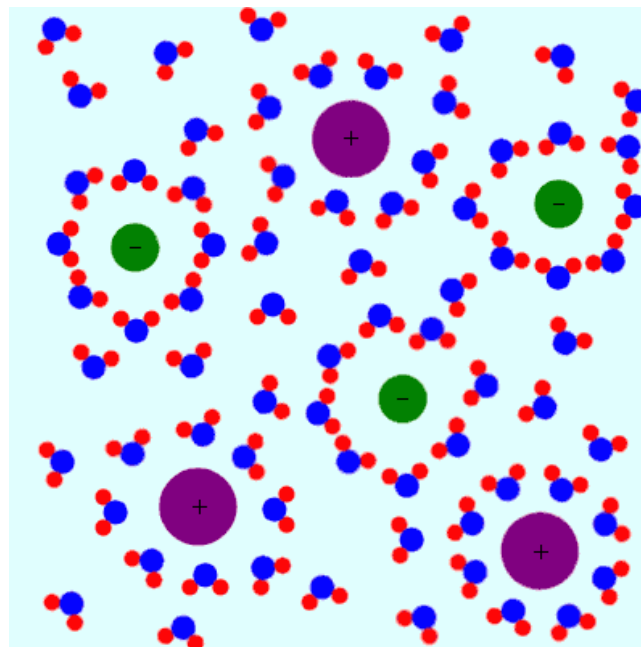


Figure 3.21: Schematic image of salt solved in water [35].

## 3.5 Xylan

### 3.5.1 Production of the xylan films

As described in chapter 2.1, xylan films are spincoated on the already existing cellulose layers. For that purpose powdery xylan is solved in DMSO (dimetyl sulfoxide) (Figure 3.22).

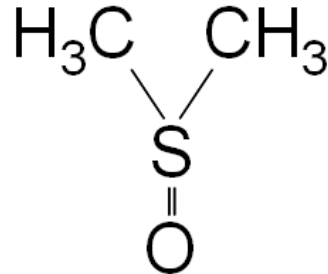


Figure 3.22: Structure of dimetyl sulfoxide (DMSO) [?]

Since DMSO is a strong polar solvent, it is possible that it solves or changes the existing cellulose layers. 3 different investigations are performed to determine the influence of the DMSO to the cellulose:

#### **Infrared spectroscopy**

DMSO is spincoated on a finished cellulose film and is investigated by RAIRS. These experiments were executed by Mario Djak and are illustrated in his master thesis [14]. The measured spectras indicate that the structure of the cellulose stays unchanged after the interaction with the DMSO.

#### **Optical investigation**

A similar prepared film is investigated by optical microscopy before and after the spincoating process (Figure 3.23). To have reference/remarkable points on the film, an inhomogenous film is used.

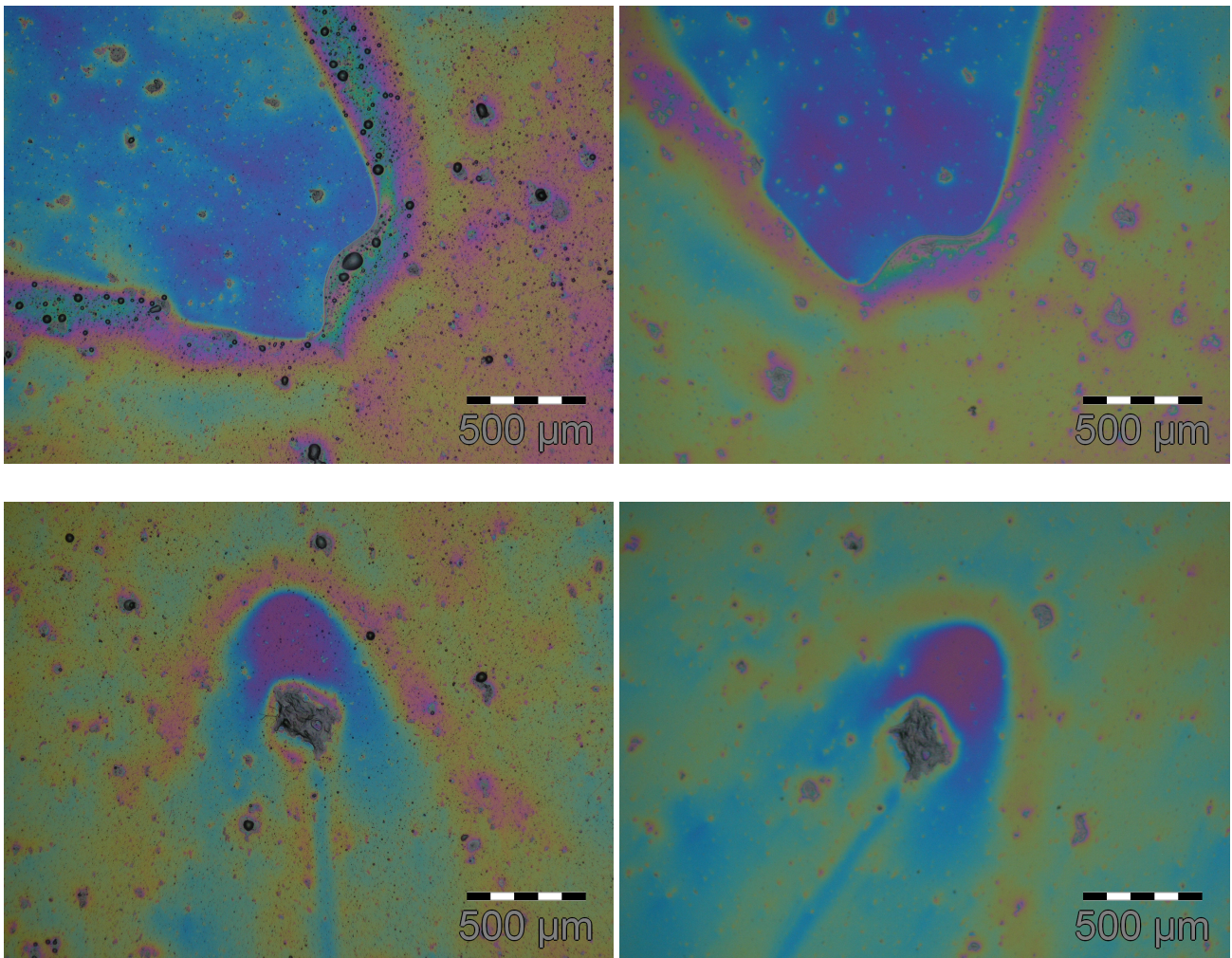


Figure 3.23: Microscopic images of the cellulose surface before (left) and after (right) spincoating with DMSO at two different striking spots.

Since the film was stored for several days, some foreign particles contaminated the surface. These particles were washed away by the DMSO during the spincoating. Although the structure of the surface seems to be unchanged, the reflexion colour, which is an indicator for the film thickness, has altered. The blue colour seems to be a little bit more dominant than before. It seems, that the DMSO solved an extremely thin and homogenous layer of the cellulose.

### Tensile tests

To analyse, if the DMSO has any influence to the filmbonding, blank tensile tests are performed. Hereby, 6 cellulose samples are prepared, as in the experiment for cellulose swelled in distilled water (3.3), only that the finished cellulose films are spincoated with DMSO. Before swelling, the samples are stored for 24 hours, so that the DMSO can evaporate away. The results are illustrated in Table 3.11 and Figure 3.24:

Table 3.11: Tensile test results of cellulose samples spincoated with DMSO.

<sup>1</sup> ... Sample is ripped apart too early → Test invalid

$F_{max} / N$	$E / mJ$
-0,0248 <sup>1</sup>	-0,0225 <sup>1</sup>
-0,8152	-0,0128
-1,7811	-0,4575
-0,4909	-0,0101
-1,9124	-0,1080
-3,1027	-0,4020

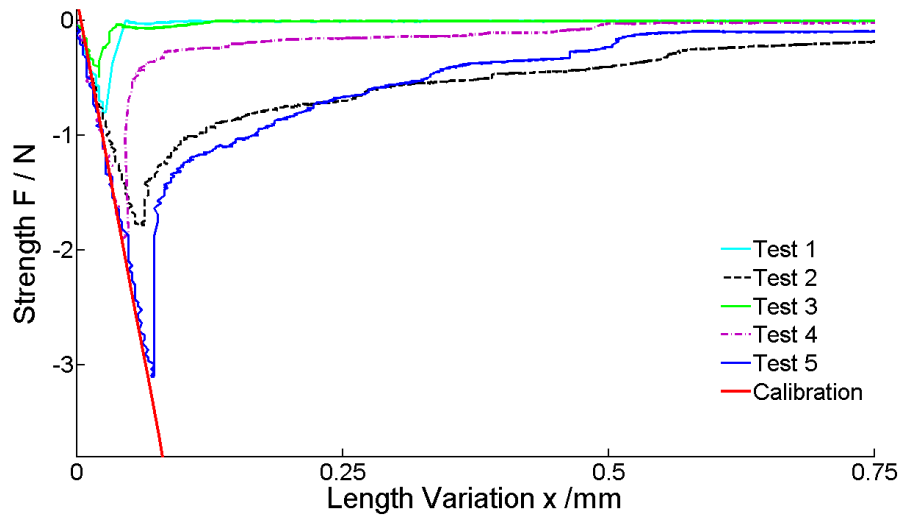


Figure 3.24: Valid tensile tests of, with DMSO spincoated, cellulose samples. Not included: Invalid test one.

The mean value for the maximum strength  $F_{max}$  and the bonding energy  $E_b$  are:

$$\bar{F}_{max} = (-1.6 \pm 1.0) N$$

$$\bar{E}_b = (5.3 \pm 5.3) \cdot 10^{-22} \frac{kJ}{nm^2}$$

In Figure 3.25 these values are compared to the results obtained for cellulose swelled in distilled water. There is no significant difference in both categories. Although, just 5 valid results could be obtained, it is an indication that the spincoating of DMSO on cellulose does not have any influence to the bonding.

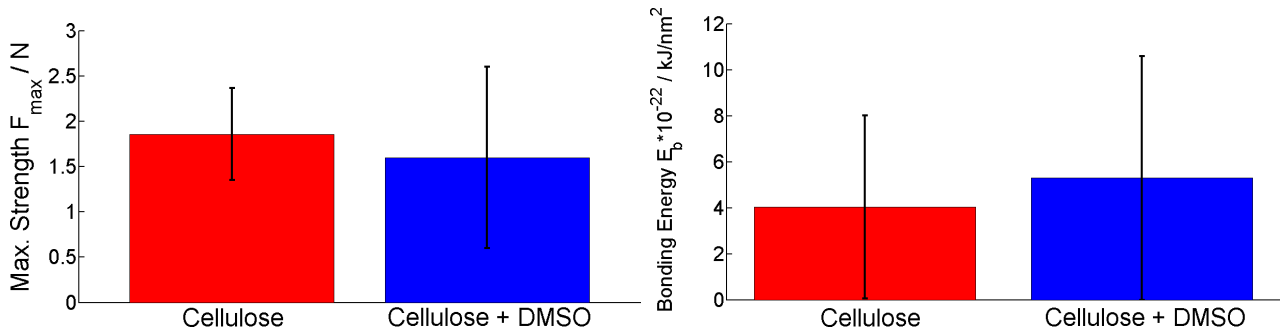


Figure 3.25: The comparison of cellulose with cellulose spincoated with DMSO. Right, the maximum strength  $F_{max}$ . Left, the bonding energy  $E_b$ . Both are swelled in distilled water.

## Result

All three measurements showed that the DMSO is not, or only slightly (in the optical investigation) changing the chemical composition and the surface character of the cellulose film. That is why, it is a good solvent choice for xylan. Further effects of the DMSO usage as a solvent are:

- The DMSO, while not changing the cellulose structure, diffuses into the film and softening it in a split of a second. So, while placing the solution on the substrate, the cellulose surface should not be touched. Otherwise, a irreversible macroscopic damage of the cellulose film is very likely.
- After spincoating, DMSO is still stored inside the films. Since it has a very high boiling point of  $189^{\circ}\text{C}$ , it needs several hours to completely evaporate [36]. That is why, the samples were stored for at least 24h before swelling.

## 3.5.2 Results

The tensile test results for xylan swelled in distilled water are imaged in Table 3.12. The data marked with <sup>1</sup> are invalid. The reasons are explained in chapter 3.3.1.

Table 3.12: Tensile test results for xylan swelled in distilled water.

1 ... Sample is ripped apart too early → Test invalid

1.Series	2.Series	3.Series
$F_{max} / \text{N}$	$F_{max} / \text{N}$	$F_{max} / \text{N}$
-2,4476	-0,8092 <sup>1</sup>	-2,1430
-1,7862	-0,9450 <sup>1</sup>	-1,9699
-1,7953	-1,1866 <sup>1</sup>	-2,2238
-2,5599	-0,1953 <sup>1</sup>	-1,1868
-2,4604	-3,2405	-1,1986
-1,5890	-1,2997	-0,8505 <sup>1</sup>
-1,0921	-1,8118	-0,5891 <sup>1</sup>
-3,1624	-2,5683	-0,0091 <sup>1</sup>
	-4,5299	-1,2483
	-2,2319	-1,5119

What stands out is, that for xylan no film detached off the silicon substrate. That is an indication, that just the xylan surfaces are interacting with each other and the influence of the cellulose to the tensile tests is small.

### 3.5.3 Calculation of the data

As for cellulose swelled in distilled water (Chapter 3.3.2), a Q-Q plot to evaluate if the results for the maximum strength  $F_{max}$  are normal distributed is used (Figure 3.26). The data points, except of one (marked by a red circle), are approximately following the red line representing perfect normal distributed data. Only the lower strength points (upper tail) show little deviation from the fitted line. That the red circled point is indeed an outlier, is proved by an outlier test after Grubb, after which it is removed from the data. To ensure that the lower strength results are not outliers, also these were examined by this test.

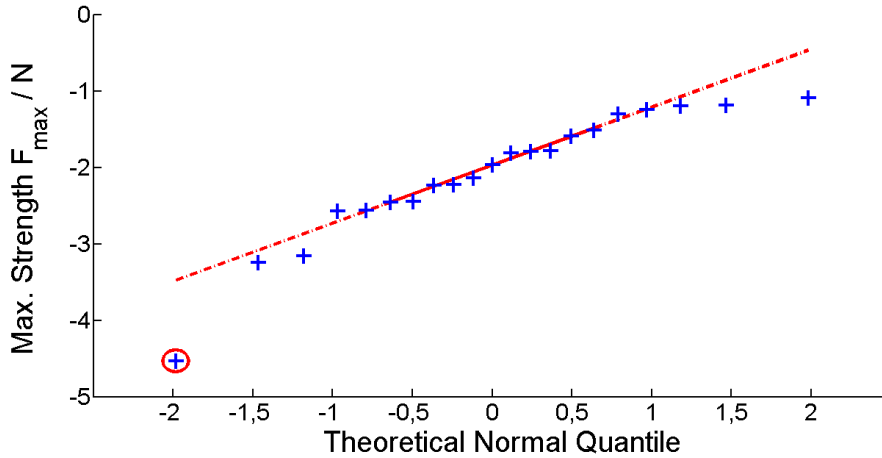


Figure 3.26: A Q-Q plot of the xylan samples swelled in distilled water. The results for the maximum strength  $F_{max}$  (blue crosses) are plotted with respect to theoretical normal quantile. The red line represents perfect normal distributed data. The incircled data point indicates a possible outlier.

The remaining results and also the calculated bonding energies  $E$  are illustrated in Table 3.13 and in Figure 3.27. The linear increase until the maximum strength  $F_{max}$  is reached varies widely for the three test series. In test series 1, the slope is steeper than the calibration curve. The only possible explanation is that the cellotapes absorbed less energy during the tests. In the test series 2 the curves have more or less the same slope as the calibration curve. The slope of the curves in the test series 3 however, is flatter than the calibration curve and some tests seem to consist of several peaks. These effects could be due to interlocking of the films. These facts are the main reason for the big deviation of the bonding energy. For further analysis the mean values and the standard deviation out of these 20 valid tests are calculated:

$$\bar{F}_{max} = (-1.98 \pm 0.64) N$$

$$\bar{E}_b = (4.4 \pm 2.2) \cdot 10^{-22} \frac{kJ}{nm^2}$$

Table 3.13: Valid tensile test results for xylan films swelled in distilled water

Nr	$F_{max}$ / N	$E$ / mJ
1	-2,4476	-0,3378
2	-1,7862	-0,1206
3	-1,7953	-0,2421
4	-2,5599	-0,1299
5	-2,4604	-0,0926
6	-1,5890	-0,1553
7	-1,0921	-0,0451
8	-3,1624	-0,0953
9	-3,2405	-0,1836
10	-1,2997	-0,0681
11	-1,8118	-0,2563
12	-2,5683	-0,2919
13	-2,2319	-0,2524
14	-2,1430	-0,1523
15	-1,9699	-0,2069
16	-2,2238	-0,3260
17	-1,1868	-0,0698
18	-1,1986	-0,1364
19	-1,2483	-0,1648
20	-1,5119	-0,1737

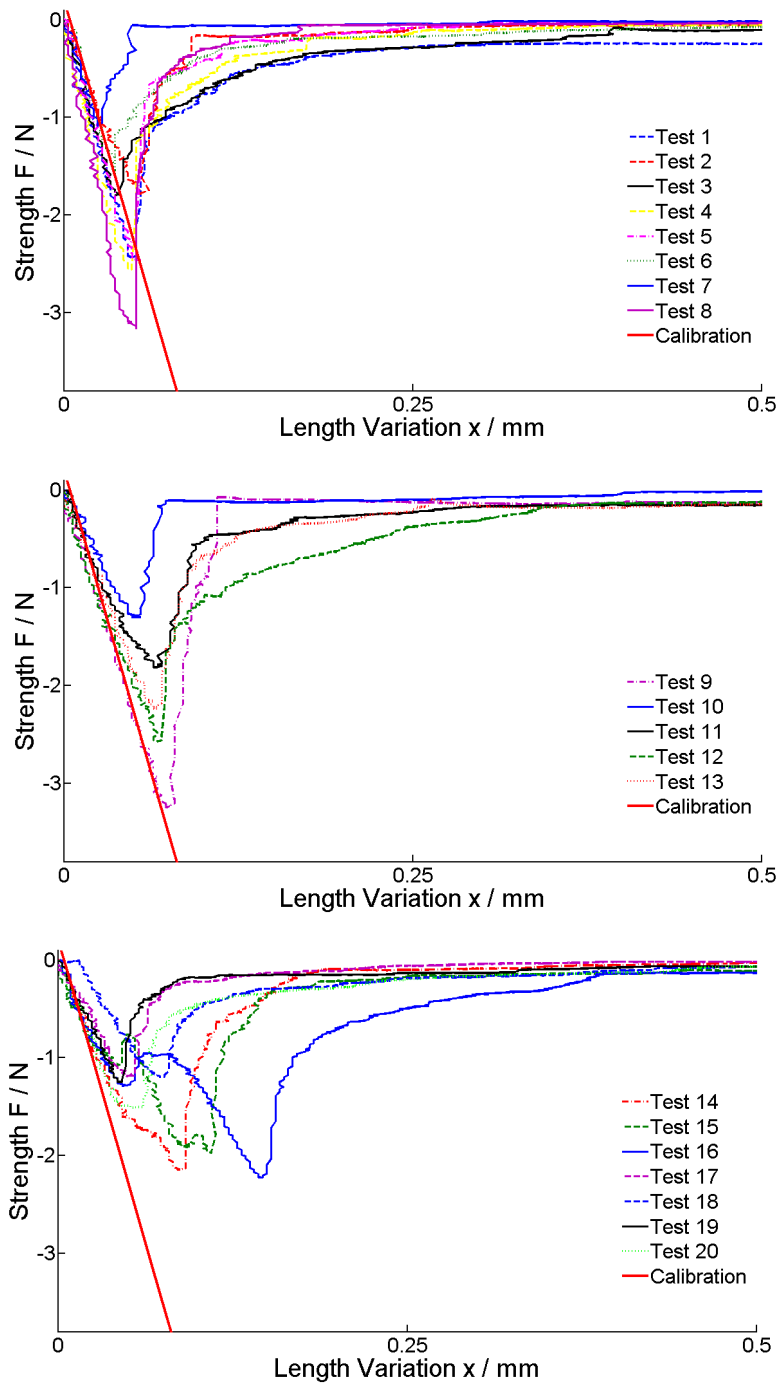


Figure 3.27: Valid tensile tests of xylan films swelled in distilled water. The force  $F$  (N) is plotted in respect to the length variation  $x$  (mm). Top-down: Test series 1, test series 2, test series 3.

### 3.5.4 Nanoindentation

A xylan film prepared in two different settings is investigated with the nanoindentation technique: Before swelling (hereafter referred to as: Dry), and right after swelling (hereafter referred to as: Wet). The wet film is always kept in the complete swelled state, by a steady water supply on the film with a pipette. The results are illustrated in Table 3.14:

Table 3.14: Nanoindentation test results for xylan.

H ... Hardness  
 $E_r$  ... Reduced modulus

Sample	H / MPa	$\Delta H$ / MPa	$E_r$ / GPa	$\Delta E_r$ / GPa
Xylan (Dry)	150	15	4,7	1,0
Xylan (Wet)	3,9	0,09	0,046	0,001

As for cellulose (Chapter 3.3.3), swelling leads to an enormous reduction of hardness and reduced modulus. The  $H_2O$  molecules, however, not only break up the hydrogen bonds, but also react with the 4-O-methyl-D-glucuronic acid sidegroup of the xylan (Equation 3.2):



In Figure 3.28 these results are compared to the results obtained for cellulose. In both cases the hardness, but also the reduced modulus (not pictured), of xylan films are significant lower. Xylan molecules compared to the cellulose molecules are mostly branched (Chapter 1.3.4). Therefore, the bulk density of the xylan is lower, which leads to less bonds and furthermore to less hardness in the dry state. This is also valid for xylan films in the wet state. Because of the lower density more water can diffuse into the bulk. In addition, as the results for xylan swelled in ionic water indicate (Chapter 3.8.2), the generated  $H_3O^+$  ions also support the swelling process.

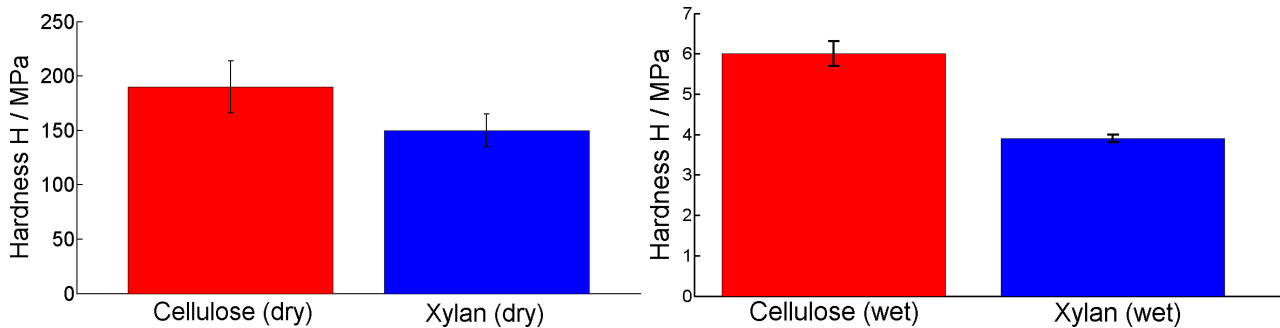


Figure 3.28: The hardness of the cellulose films is compared to hardness of the xylan films. Left in the dry state, right in the wet state.

### 3.5.5 Comparison to cellulose

In Figure 3.29 the maximum strength  $F_{max}$  and the bonding energy  $E_b$  of xylan is compared to cellulose. Although the better swelling properties of the xylan would indicate an increase in molecular contact and, therefore, bonding strength, no such thing is measured. A performed t-test for normal distributed data with an significance level of  $\alpha=0.01$  displays no significant difference in strength or energy.

According to [37] spincoating xylan on existing cellulose films leads to an increase in RMS(Root-Mean-Square) roughness  $\sigma$  and in the lateral correlation length  $\xi$ . Rougher surfaces lead to less molecular contact during bonding.

In conclusion, it seems that the better swelling properties and the rougher surfaces are cancelling each other out. In total, around the same amount of molecular contact area is created for xylan films as cellulose films.

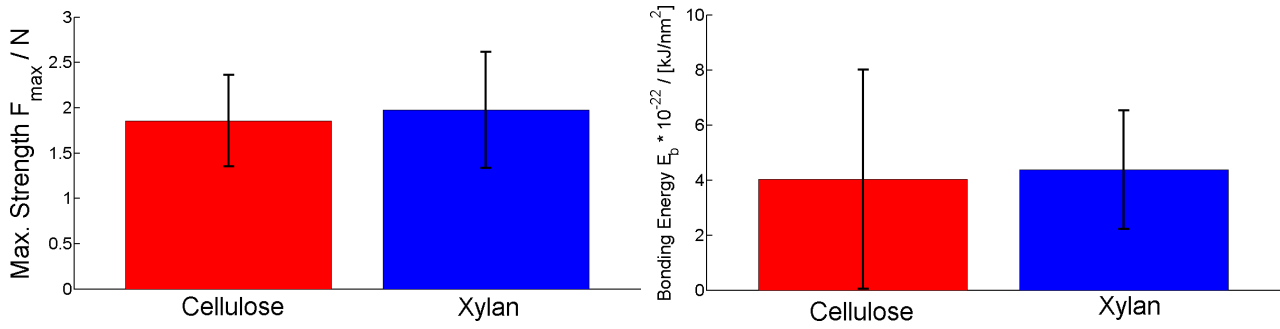


Figure 3.29: Comparison of the maximum strength  $F_{max}$  (N) (right) and the bonding energy  $E_b$  ( $\frac{kJ}{nm^2}$ ) of xylan with cellulose (left). Both results are obtained for swelling in distilled water.

### 3.6 Cellulose-Xylan

The tensile tests results for mixed samples (one side cellulose, the other xylan) swelled in distilled water are illustrated in Table 3.15.

Table 3.15: Tensile tests results for cellulose-xylan samples (mixed samples) swelled in distilled water.

- 1 ... Series invalid
- 2 ... Sample is ripped apart too early → Test invalid

1.Series <sup>1</sup>	2.Series	3.Series
$F_{max} / N$	$F_{max} / N$	$F_{max} / N$
-1,3734	-2,8590	-4,2526
-0,7046	-2,2977	-2,2821
-1,2222	-1,4923	-2,8314
-2,0832	-4,2786	-0,0787 <sup>2</sup>
-1,8950	-3,5879	-1,8739
-0,6629	-3,4804	-2,7613
	-3,9052	-4,4563
	-3,0531	-4,4104
	-3,9218	-3,4903
		-9,4191
		-2,7265

Due to reservation issues, the swelling time in the first test series (marked with <sup>1</sup>) was only 4h, 9h shorter than for the other series. Because of that, especially the cellulose films were not perfectly swollen, and therefore, the results are significantly lower. The test marked with <sup>2</sup> is invalid, because the sample ripped apart in the pressure area (more precise explanation in chapter 3.3.1).

#### 3.6.1 Calculation

In Figure 3.30 the Q-Q plot for the obtained results is illustrated. The results for the maximum strength (blue crosses) are indeed again normal distributed, by following the red line indicating

perfect normal distributed data. The point marked with a red circle seems to be an outlier. This hypothesis is confirmed by a performed outlier test after Grubbs. That is why this data point can be removed.

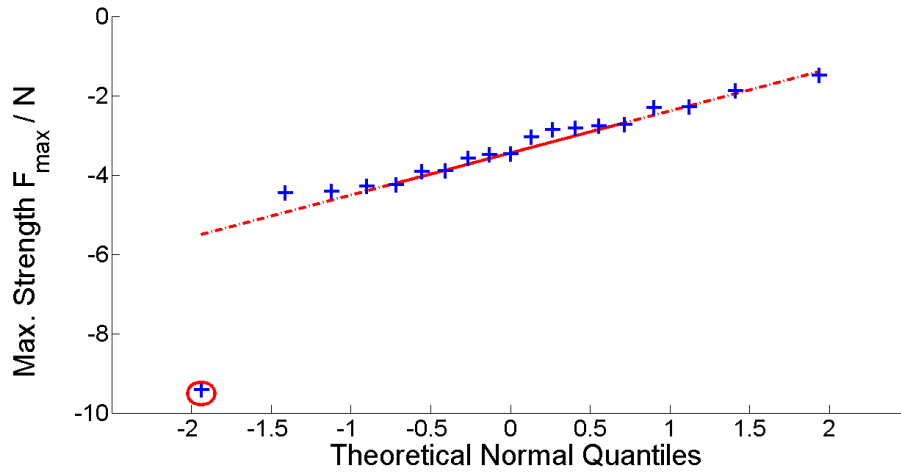


Figure 3.30: A Q-Q plot of the mixed samples swelled in distilled water. The blue crosses ( $F_{max}$ ) are the experimental results, the red line represents perfect normal distributed data.

Eventually, after removing all the invalid data, in total 18 tests, illustrated in Table 3.16 and in Figure 3.31, are at hand for further calculation. The calculated mean values and the standard derivations of the maximum strength  $F_{max}$  and the bonding energy  $E_b$  are:

$$\bar{F}_{max} = (-3.22 \pm 0.90) N$$

$$\bar{E}_b = (11.6 \pm 7.6) \cdot 10^{-22} \frac{kJ}{nm^2}$$

Table 3.16: Valid tensile test results for the mixed samples swelled in distilled water.

$F_{max}$  ... Maximum strength

E ... Bonding energy

Nr	$F_{max}$ / N	E / mJ
1	-2,8590	-0,9098
2	-2,2977	-0,6527
3	-1,4923	-0,1631
4	-4,2786	-1,0364
5	-3,5879	-0,5773
6	-3,4804	-0,7883
7	-3,9052	-1,2351
8	-3,0531	-0,5910
9	-3,9218	-0,4968
10	-4,2526	-0,6859
11	-2,2821	-0,5654
12	-2,8314	-0,3816
13	-1,8739	-0,2876
14	-2,7613	-0,6414
15	-4,4563	-1,2175
16	-4,4104	-0,6980
17	-3,4903	-0,7887
18	-2,7265	-0,2542

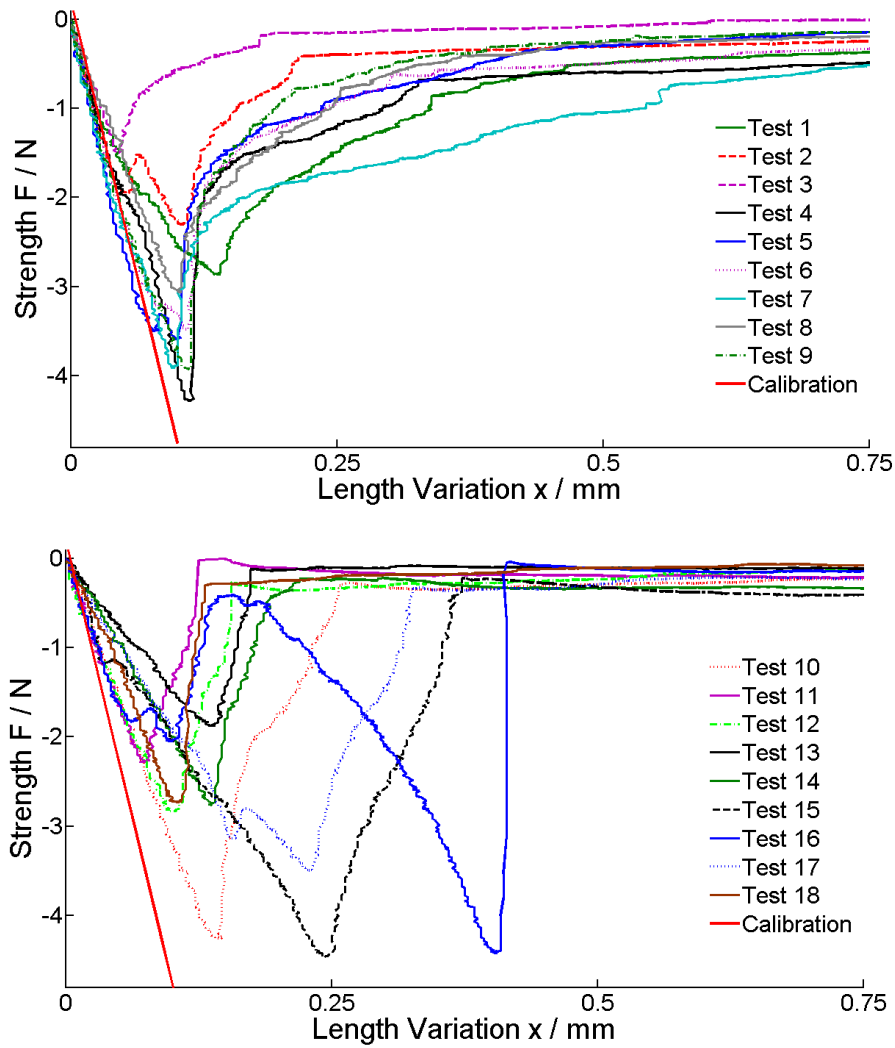


Figure 3.31: Valid tensile tests of the in distilled water swelled cellulose-xylan samples. The force  $F$  (N) is plotted in respect to the length variation  $x$  (mm). Top-down: Test series 2 and 3.

### 3.6.2 Comparison of the results obtained to cellulose and xylan

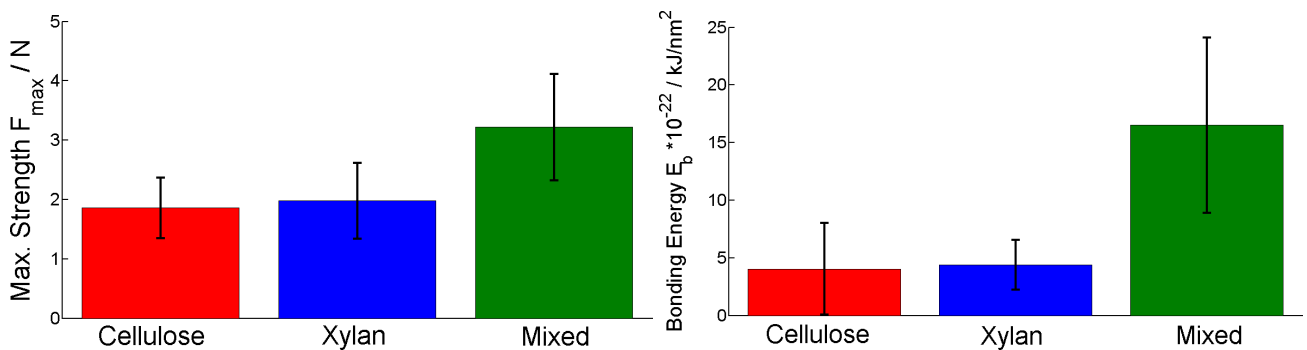


Figure 3.32: Comparison of the results for cellulose and xylan swelled in distilled water, with the results obtained for mixed samples. The left histogram shows the values for the maximum strength  $F_{max}$ , the right one for the bonding energy  $E_b$

In figure 3.32 the obtained values are compared with the experimental results for cellulose and xylan samples, both swelled in distilled water. A performed t-test for comparing mean values, shows a significant increase in both maximum strength and bonding energy at a significant level of  $\alpha = 0.01\%$ .

It seems, that the good swelling properties of the xylan and the smoother surface of the cellulose prove to be a good combination and leads to a big contact area. As explained in chapter 3.3.3, the amount of Van-der-Waal and hydrogen bonds and, therefore, the bonding strength, is directly proportional to the area in molecular contact.

### 3.7 Xylan with dimethyl sulfoxide (DMSO)

Dimetyl sulfoxide is not completely flying of the substrates edges or evaporates during the spincoating process. Instead, it remains on the substrate and diffuses into the already existing cellulose layers. The polar solvent breaks up the hydrogen bonds and therefore, soften the film. In the investigation of xylan samples the films are dried in a flow box for at least 24h, so that the DMSO can evaporate away. During that process the hydrogen bonds establish again and the influence of the DMSO vanishes (Chapter 3.5.1).

If the samples are put into water for swelling right after spincoating, the solvent is still inside and the hydrogen bonds are already broken. The question is, if this influences the swelling behaviour and, therefore, the film bonding strength.

Table 3.17: Tensile test results for xylan with stored DMSO swelled in distilled water (xylan+DMSO).

1. Series		2. Series	
$F_{max}$ / N	E / mJ	$F_{max}$ / N	E / mJ
-4,3113	-0,6000	-4,5206	-0,2255
-3,8451	-0,5597	-5,2062	-0,1448
-2,7736	-0,6302	-4,0539	-0,4232
-1,5370	-0,4773	-4,4907	-0,4170
-1,7747	-0,1811	-4,4196	-0,3241
-3,4153	-0,5596	-3,9962	-0,0484
-3,3898	-0,7588	-6,6961	-0,1671
-3,3339	-0,4901	-2,1314	-0,1370
-2,9708	-0,3053	-1,8694	-0,0821
-2,7945	-0,4418		

In Table 3.17 the tensile test results for xylan+DMSO (xylan with stored DMSO) swelled in distilled water is illustrated. More experience in film production and in the usage of the power rheometer, leads to 19 test results, where none showed any invalid behaviour. That is why, also the bonding energies are illustrated in Table 3.17. In the first test series the samples were put into the water 1h after spincoating. In the second test series right after spincoating. By comparing the mean value  $\bar{F}_{max}$  of both series, one can determine if that change in routine had any influence to the experiments:

$$\begin{aligned}
 1.Series : \quad \bar{F}_{max1} &= (-3,02 \pm 0,86) N \\
 2.Series : \quad \bar{F}_{max2} &= (-4,15 \pm 1,47) N
 \end{aligned}$$

Although the second series has a higher mean value, the difference is not significant. That is why the two test series are identical.

### 3.7.1 Calculation

Figure 3.33 shows the Q-Q plot for  $F_{max}$ . The blue crosses, which indicate the experimental results seem to be normal distributed. Furthermore no outlier could be identified, which is proved by an outlier test after Grubbs. Since no results were eliminated, all performed 19 tensile tests can be used for further calculations and comparisons.

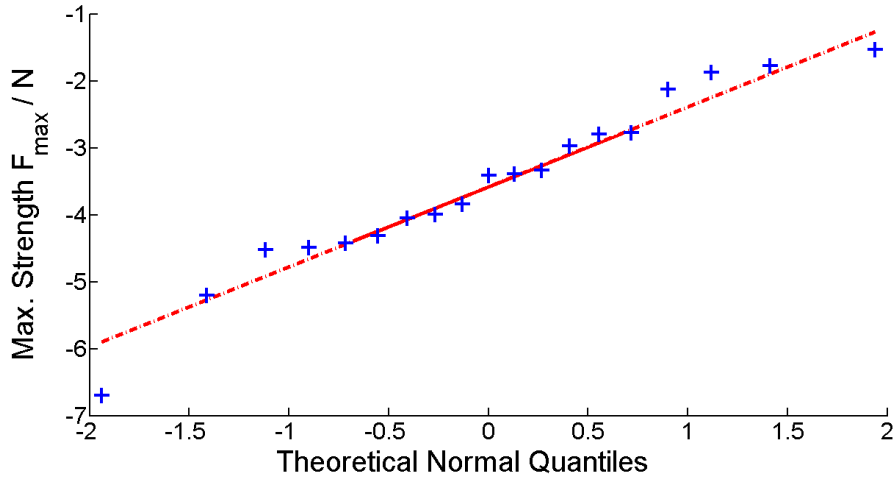


Figure 3.33: Q-Q plot of the xylan+DMSO samples. The maximum strength  $F_{max}$  (blue crosses) is plotted in respect to the theoretical normal quantile. The red line indicates perfect normal distributed data.

The mean values of the maximum strength and the bonding energy, which are illustrated in Figure 3.34 are:

$$\bar{F}_{max} = (-3, 55 \pm 1, 29) N$$

$$\bar{E}_b = (9, 2 \pm 5, 2) \cdot 10^{-22} \frac{kJ}{nm^2}$$

The two test series possess a completely different slope in the linear area. Especially the slopes in the second test series are steeper than the slope of the calibration curve. That indicates that the slope of the cellotapes seems to vary. Furthermore, although  $\bar{F}_{max}$  is smaller for the first series than for the second series, the bonding energies are bigger, since the strength of the samples in the second series is dropping to nearly zero, right after the maximum strength point is reached.

Hence, in first test series the films just partly separated at the maximum strength point and therefore still needed energy to separate the still bonded area. On the other hand, the films in the second test series separated at once, that is why no more energy is needed. That is also the reason for the higher maximum strength. This is another indicator that although the two test series look different, they have actually the same amount of formed Van-der-Waals and hydrogen bonds. In the first they just broke over the time, at the second at once.

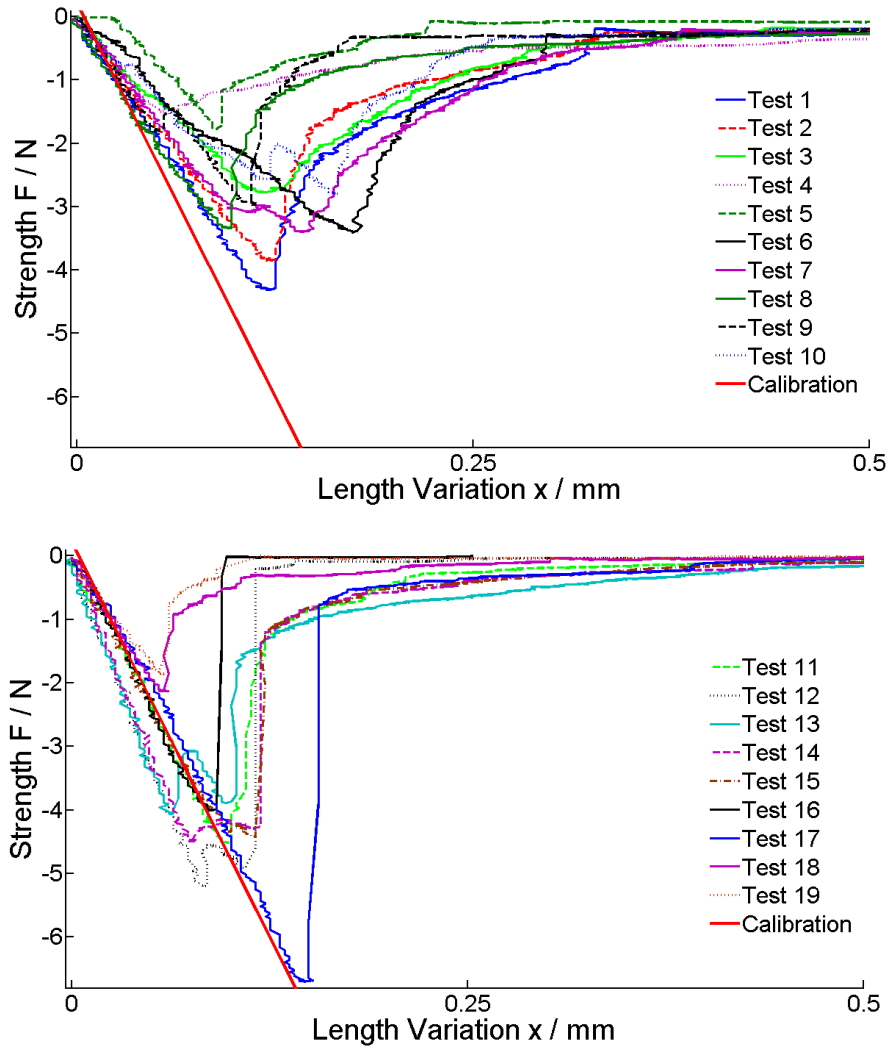


Figure 3.34: Valid tensile tests of the in distilled water swelled xylan+DMSO samples. The force  $F$  (N) is plotted in respect to the length variation  $x$  (mm).

### 3.7.2 Comparison of the results to xylan

In Figure 3.35 the maximum strength and the bonding energy of xylan and xylan+DMSO are compared to each other. A t-test for comparing mean values shows a significant increase in both categories at a significant level of  $\alpha = 0.01\%$ .

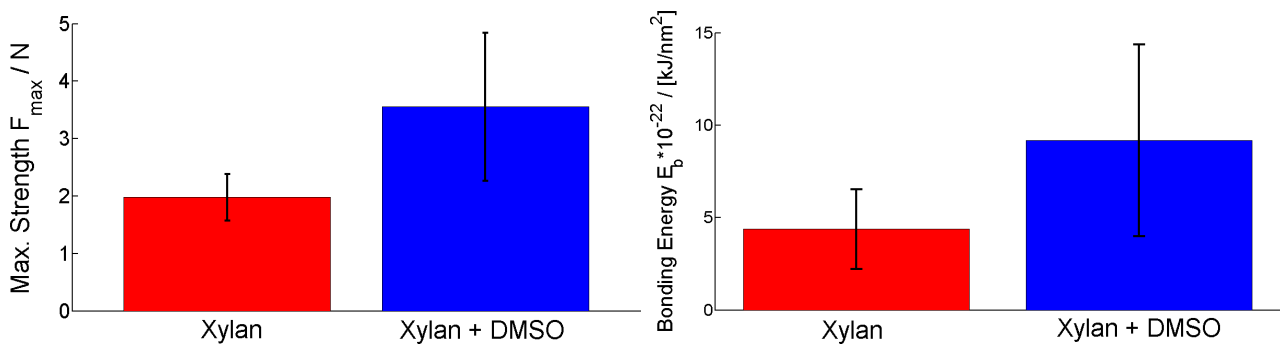


Figure 3.35: Comparison of xylan with xylan+DMSO, both swelled in distilled water. Left the maximum strength  $F_{max}$ , right the bonding energy  $E_b$

## Nanoindentation

The hardness  $H$  and the reduced modulus  $E_r$  for a xylan+DMSO film, swelled in distilled water are:

$$H = (3.4 \pm 0.2) \text{ MPa}$$
$$E_r = (0.033 \pm 0.0013) \text{ GPa}$$

In figure 3.36 these results are compared with the results obtained for xylan samples swelled in distilled water.

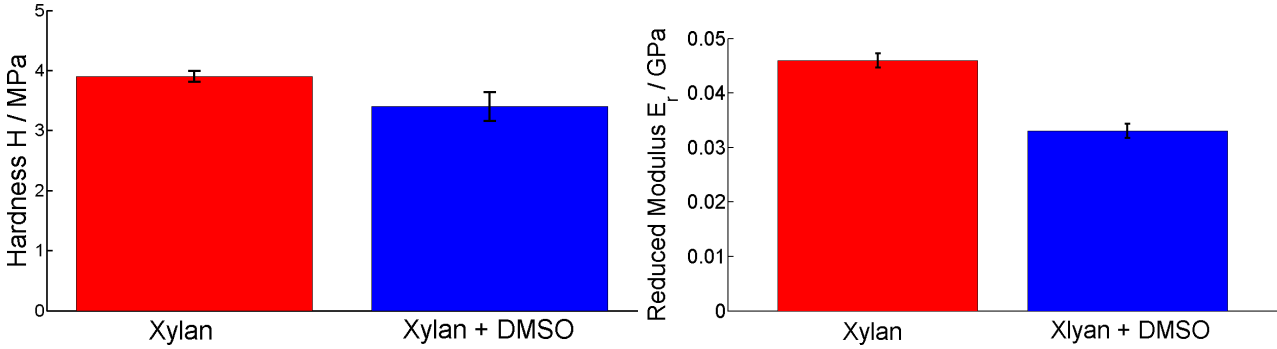


Figure 3.36: Hardness-Comparison of a xylan-film with a xylan-DMSO film .

The hardness for the xylan+DMSO films is significant lower than for the xylan films. For the reduced modulus  $E_r$ , this difference is even bigger. In the comparison of xylan to cellulose (Chapter 3.5.5), the effect of the softer films seems to be canceled out by the rougher surface. For xylan+DMSO it appears that the reduced hardness is starting to dominate, which transpires in an increase of area in molecular contact and with that in an increase of bonding strength and energy compared to xylan and cellulose.

## 3.8 Xylan swelled in ionic water

Xylan is swelled in water containing  $0.1 \frac{\text{mol}}{\text{l}} \text{ CaCl}_2$ . The salt dissolves in the water into  $\text{Ca}^{2+}$  and  $\text{Cl}^-$ . The positiv calcium ions (cations) should be able to form ionic bonds with the negative charged acide groups (Equation 3.2).

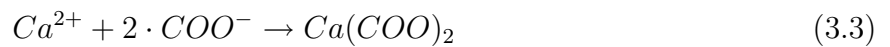


Table 3.18: Tensile test results for xylan films swelled in ionic water.

Nr	1.Series			2.Series		
	$F_{max}$ / mJ	E / mJ	Type	$F_{max}$ / N	E / mJ	Type
1	-2,7681	-0,8818	3	-0,6291	-0,0508	2
2	-4,6211	-1,7129	3	-17,2193	-1,2532	4
3	-1,3352	-0,3663	2	-4,5062	-0,4434	1
4	-4,2224	-1,4045	3	-11,1187	-3,0315	3
5	-0,2200	-0,3218	3	-12,7422	-1,8705	4
6	-0,2745	-0,1484	1	-13,0879	-2,7885	3
7	-4,4890	-1,8929	3	-10,4650	-3,2128	3
8	-0,9238	-0,2297	1	-13,3766	-4,0538	3
9	-0,9117	-0,3958	1	-6,2207	-2,0152	3
10	-7,7930	-2,1897	4	-3,2087	-0,3703	1
11	-4,2660	-2,6025	3	-4,1126	-0,3760	1
12				-7,1760	-2,2873	2
13				-10,4814	-2,6425	4
14				-3,1086	-0,3188	1

In total 2 test series with each 11 and 14 tests, illustrated in Table 3.18, were executed. These tests were performed by Michael Klemm in the course of his bachelor thesis [38]. Not all of the samples separated between the desired xylan-xylan layers. The ,with ‘‘Type’’ labeled numbers 1 to 4, define between which layers the samples actually separated:

1. As desired, the films separated between the two xylan surfaces.
2. Sample partly separated between the xylan films and partly between other layers.
3. Sample completely separated between other layers.
4. One cellotape detached before the sample was separated.

The mean values and the standard deviations of the maximum strength  $F_{max}$  and the bonding energy  $E_b$  for the two test series are:

1.Series:

$$\bar{F}_{max1} = (-2.89 \pm 2.40) N$$

$$\bar{E} = (27.6 \pm 22.2) \cdot 10^{-22} \frac{kJ}{nm^2}$$

2.Series:

$$\bar{F}_{max2} = (-8.40 \pm 4.20) N$$

$$\bar{E} = (44.1 \pm 32.5) \cdot 10^{-22} \frac{kJ}{nm^2}$$

Because of more experience in the film production, the samples in the second test series are bonding stronger than in the first one. That is why, in further calculations and analysis just the second series is used.

### 3.8.1 Calculation

To evaluate, if the results for the maximum strength  $F_{max}$  are normal distributed a Q-Q plot is used (Figure 3.26). It turns out, that different to all other settings, these results are not fitted by the red line representing normal distributed data. Especially the results in the high strength region are deviating, because hereby the cellotape or other layers yielded before the samples could separated between the desired xylan surface. That is why, it is not allowed to used the Grubb test to identify outliers, since this test requires normal distributed data. So, all tests of the second test series, illustrated in Figure 3.38 are valid and the mean values calculated above are hereby correct.

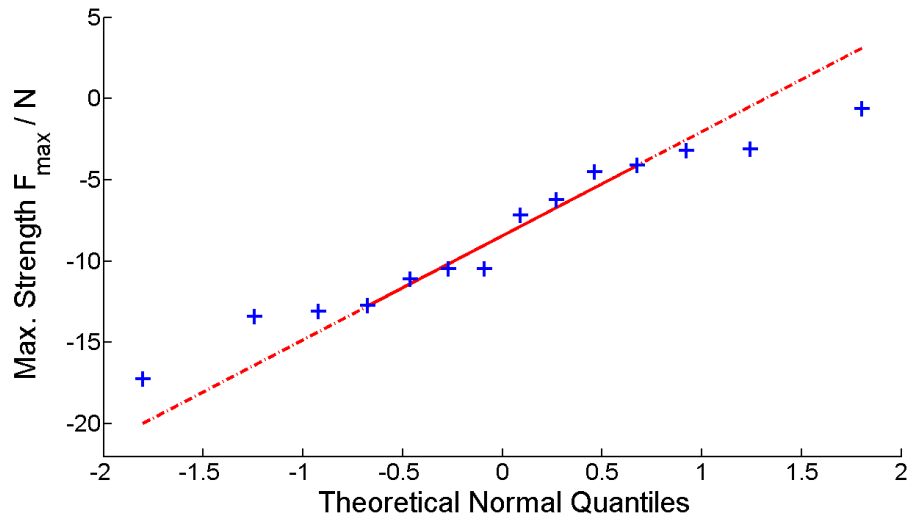


Figure 3.37: Q-Q plot of xylan sample swelled in water containing  $CaCl_2$ . The results for the maximum strength  $F_{max}$  (blue crosses) are plotted in respect to the theoretical normal quantile. The red line is representing perfect normal distributed data.

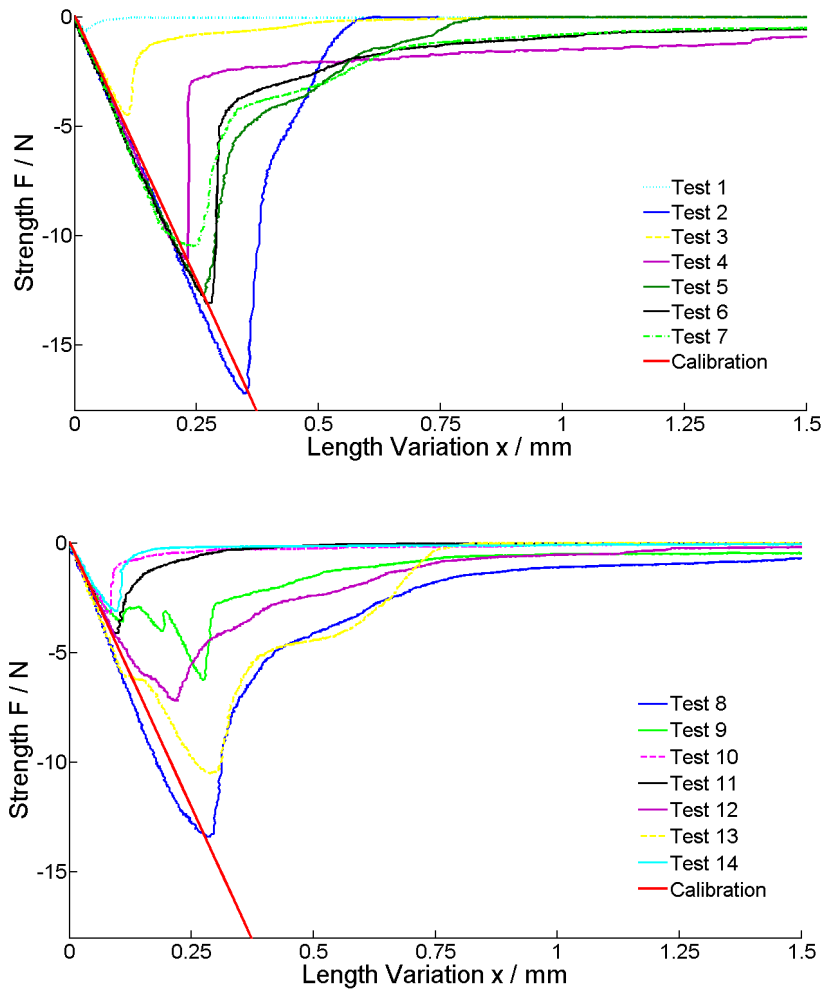


Figure 3.38: Valid tensile tests of the xylan films swelled in water containing  $CaCl_2$ . Top-bottom: Tests 1-7 and 8-14 of the second test series.

### 3.8.2 Comparison with other settings

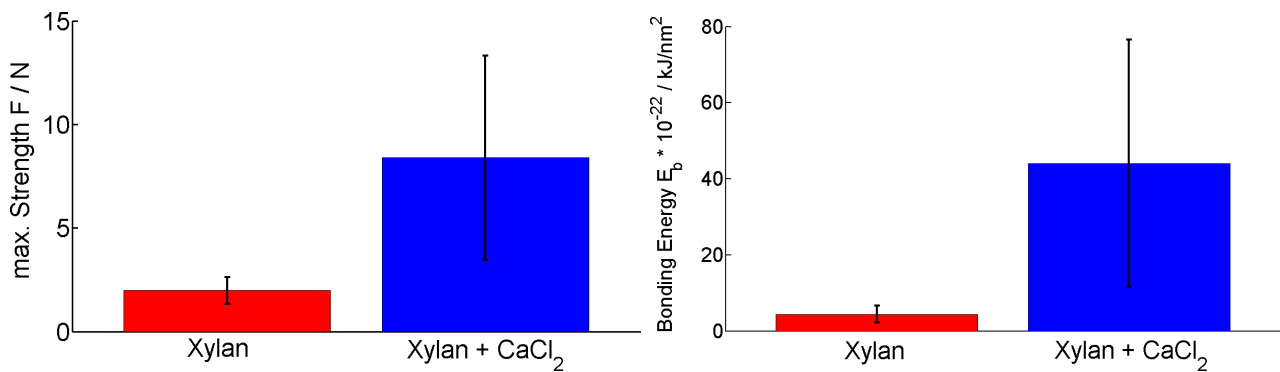


Figure 3.39: Comparison of xylan swelled in distilled water with xylan swelled in ionic water. Left, the maximum strength  $F_{max}$  (N), right the bonding energy  $E_b$  ( $\frac{kJ}{nm^2}$ )

In Figure 3.39, the obtained results are compared to the results for xylan swelled in distilled water. Since the data are not normal distributed it is not allowed to use a t-test for comparing mean values. Nevertheless, the obtained results indicate a strong increase in strength and bonding energy. Furthermore, since some samples dissolved between different layers, they might be even higher. Two main reasons for this increase are explained in the following subchapters:

## Nanoindentation

A xylan film swelled in water containing  $CaCl_2$  (wet state), is investigated with the nanoindentation technique. The hardness  $H$  and the reduced modulus  $E_r$  are:

$$H = (3.5 \pm 0.1) \text{ MPa}$$

$$E_r = (0.042 \pm 0.001) \text{ GPa}$$

In Figure 3.40 the hardness is compared to xylan swelled in distilled water and to xylan swelled with DMSO. The results indicate, that ions are helping in the swelling of xylan. That is completely contrary to cellulose swelled in ionic water, which resulted in an increase of hardness (Chapter 3.4).

A decrease in hardness leads to an increase in area in molecular contact and furthermore, to stronger bonding. The decrease in hardness is in the same range than for xylan+DMSO. The increase in bonding strength, which can be classified to this effect, can be assumed to be roughly the same.

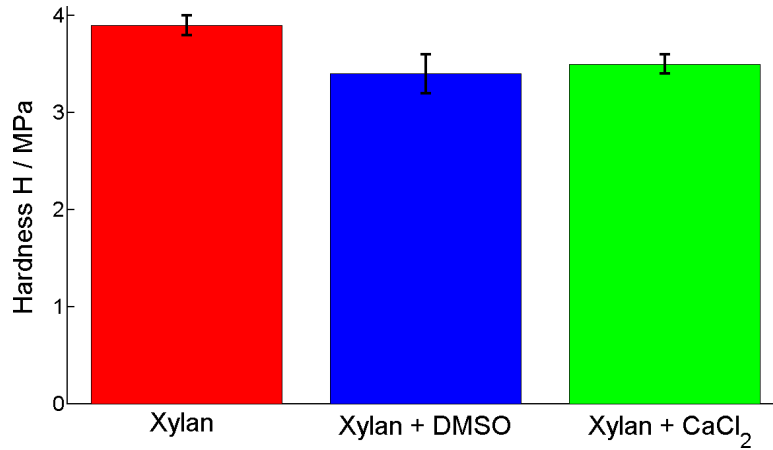


Figure 3.40: Hardness comparison of xylanfilms swelled in distilled and swelled in ionic water.

## Contribution of ions

Therefore, the greater part of the increase in strength can be credited to Coulomb interaction. Two possible configurations between two films are illustrated in Figure 3.41. Since an increase in strength could be observed, the attractive configuration b) seems to be more favoured. Nevertheless, since the results are greatly diverging and some samples showed quite small bonding strengths, the configuration a) might also occur.

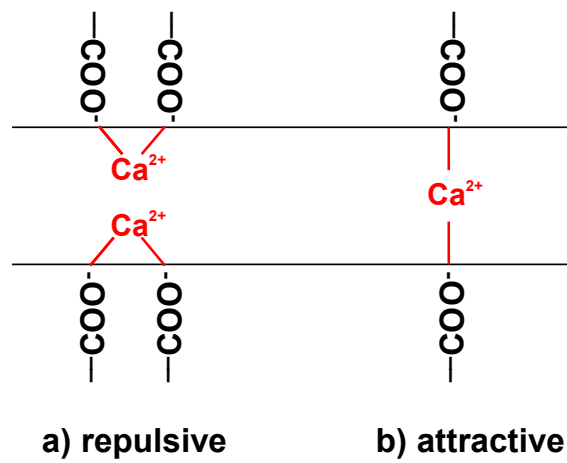


Figure 3.41: Illustration of possible Coulomb interactions between two xylan films swelled in  $CaCl_2$  water. a) Repulsive configuration; b) Attractive configuration

# Chapter 4

## Summary

The maximum strength  $\bar{F}_{max}$  and the bonding energy  $\bar{E}_b$  of two bonded films were determined in six different settings. Table 4.1 shows the relevant obtained data. Settings 1, 3, 4 and 5 are swelled in distilled water, settings 2 and 6 are swelled in ionic water (containing  $0.1 \frac{mol}{l}$   $CaCl_2$ ) to examine the influence of ions to the bonding. Furthermore, the swelling behaviour of different film configurations are investigated by the AFM using nanoindentation. The results are illustrated in Table 4.2. The films are examined before swelling (dry) and right after swelling (wet), whereby the films are kept in the completely swelled state by a steady supply of water.

Although the standard deviation of the bonding energy for setting 1 is large, the fact that it is in the range of the energies predicted by [16] shows that this model is providing good, reproducible results. To get an idea about the actual area in molecular contact, the cellulose film roughness was investigated with an AFM before and after the tensile test. The results are illustrated in Table 3.8. The RMS (root mean square) roughness is more or less halved after the tensile test compared to before. This indicates that during bonding the films get plastically deformed and form a big area in molecular contact. The reason for this deformation is the dramatical reduce in hardness  $H$  and reduced modulus  $E_r$  because of swelling. During bonding the soft films get pressed together by capillary forces and therefore, deform plastically [19]. Moreover, during swelling the thickness of the films is increasing up to a ratio of  $\sim 1.6 \frac{d}{d_0}$  in only 30min.

The bonding strength of cellulose films swelled in ionic water (setting 2) is significantly lower than for setting 1, which is proven by a t-test. That indicates that no Coulomb bonds are formed between the added ions and the cellulose molecules. Furthermore, it results in a worsening of the swelling behaviour (increased hardness  $H$  and reduced modulus  $E_r$ ), which leads to a decreased area in molecular contact between the two films. The amount of Van-der-Waals and hydrogen bonds depends on this area and therefore, explains the reduction in strength.

The influence of xylan to fibre-fibre bonding is investigated in the settings 3-6. Although the hardness in the dry and in the wet state of xylan is significantly reduced compared to cellulose, no significant increase, proven by a t-test, could be measured by comparing setting 1 with xylan swelled in distilled water (setting 3). The reason that the better swelling is not resulting in bigger area in molecular contact is that the xylan film surfaces are significantly rougher. Therefore, these two effects are cancelling each other out. The significant increase in both strength and energy for setting 5 compared to setting 3 shows that the swelling behaviour is crucial to bonding. Hereby the films are put in water for swelling right after spincoating. That is why, the solvent dimethyl sulfoxide (DMSO) is still incorporated in the film bulk. This results in less hardness in the wet state, or to be precise, to better swelling. Since all the other

parameters are kept identical, the increase in strength and energy can be attributed to the area in molecular contact and therefore, to the better swelling properties. Also the mixed sample tests (Setting 4. Xylan-Cellulose) show a significant increase in both categories. It seems the good swelling behaviour of the xylan and the less rough surface of the cellulose are a good combination.

By adding ions to swelling of the xylan films (setting 6) it is possible to investigate the interaction of cations with the acide sidegroup of the xylan. Two possible configurations are illustrated in Figure 3.41. The tensile test results show a dramatic increase, especially for the bonding energy. One big problem was that some samples seperated between other film layers or before the maximum strength was reached the cellotapes detached of the cylinders. Therefore, the maximum mean values might be higher and the standard deviations smaller. In addition to the attractive Coulomb interactions, the salt is leading to better swelling, which leads to a superposition of these two positive effects.

Table 4.1: Results of the tensile tests

$\bar{F}_{max}$  ... Mean value of the maximum strength  
 $\bar{E}_b$  ... Mean value of the bonding energy

Setting	$\bar{F}_{max}$ / N	$\bar{E}_b \cdot 10^{-22}$ / $\frac{kJ}{nm^2}$
1. Cellulose - Cellulose	$-1.86 \pm 0.51$	$4.0 \pm 4.0$
2. Cellulose - Cellulose + CaCl <sub>2</sub>	$-1.10 \pm 0.43$	$4.4 \pm 2.2$
3. Xylan - Xylan	$-1.98 \pm 0.64$	$4.4 \pm 2.2$
4. Xylan - Cellulose	$-3.22 \pm 0.90$	$11.6 \pm 7.6$
5. Xylan - Xylan + DMSO	$-3.55 \pm 1.29$	$9.2 \pm 5.2$
6. Xylan - Xylan + CaCl <sub>2</sub>	$-8.40 \pm 4.20$	$44.1 \pm 32.5$

Table 4.2: Nanoindentation results of different film settings

H ... Hardness  
 $E_r$  ... Reduced Modulus

Setting	H / Mpa	$E_r$ / GPa
Cellulose dry	$190 \pm 24$	$6.3 \pm 1.0$
Cellulose wet	$7.7 \pm 0.5$	$0.056 \pm 0.002$
Cellulose +CaCl <sub>2</sub> wet	$6.0 \pm 0.3$	$0.063 \pm 0.003$
Xylan dry	$150 \pm 15$	$4.7 \pm 1.0$
Xylan wet	$3.9 \pm 0.1$	$0.046 \pm 0.001$
Xylan + CaCl <sub>2</sub> wet	$3.5 \pm 0.1$	$0.042 \pm 0.001$
Xylan + DMSO wet	$3.4 \pm 0.2$	$0.033 \pm 0.001$

## 4.1 Outlook

In the tensile tests for xylan swelled in ionic water ( $0.1 \frac{mol}{l}$ ) the two films often bonded stronger than the film bulk or the cellotapes. Therefore, the measured values are too small. Possible solutions are:

- By taking NaCl instead of CaCl<sub>2</sub> the strength of the interactions could be narrowed, since Coulomb forces depend on the amount of charge of an atom (Na<sup>+</sup> instead of Ca<sup>2+</sup>).
- To prevent the detaching of the cellotapes a different, stronger cellotape can be used. Alternatively it might be also a good idea to change, for future experiments, the tensile test equipment.

The values for the bonding energy diverge quite strong from each other. One main reason is the inhomogeneity of the cellotapes energy absorbtion. It seems to vary strongly from one test series to another. It would be advisable to make every time a few reference measurements and make a calibration for every test series. A better possibility is to use a different, more usable sample fastening.

Since the model system is providing good and reproducible results the following experiments are of interest for further investigations of the fibre-fibre bonding:

- To investigate the area in molecular contact, it is possible to press the films during bonding with a defined force together. A possible method is measuring the bonding strength and energy as a function of the pressing force. Hereby it might be possible to determine, at what force a complete area in molecular contact is established. Furhermore, this would be an option to sepearate the influence of swelling and the influence of the Coulomb interactions for xylan swelled in ionic water. Again the bonding strength and energy would be measured as function of the pressing force, while the salt concentration would remain constant.

An easier alternative would be to change the roughness of the films. That can be done easily by changing the TMSC to Toluol ratio.

- It is possible to measure the influence of the pH-value to bonding. The easiest way is to change the pH of the water. Also nanoindentation tests of these films in the swelled state would be of interest.
- The roughness change during the bonding and unbonding of the sample is an indicator for the area in molecular contact. In this work, the roughness of only one cellulose sample was investigated by an AFM. By investigating the roughness for other settings, comparable values can be obtained.
- Since cellulose has not only amorphous but also crystalline regions in paper fibres, a possibility to make this ideal model system more realistic is to use crystalline cellulose films and mixed crystalline, amorphous films.

# Bibliography

- [1] About.com; *History of Paper-Making* (24.07.2012);  
URL: <http://inventors.about.com/od/pstartinventions/a/papermaking.htm>
- [2] P. F. Tschudin; *Grundzüge der Papiergeschichte*; Hiersemann-Verlag (2002)
- [3] Paperindustry; *Kraft Process* (24.07.2012);  
URL: <http://www.paperindustry.com/kraft-process.asp>
- [4] austropapier.at; *Internationale Zahlen 2010* (28.08.2012)  
URL: [http://www.austropapier.at/uploads/media/0\\_Internationale\\_Zahlen.pdf](http://www.austropapier.at/uploads/media/0_Internationale_Zahlen.pdf)
- [5] H. Sixta; *Handbook of Pulp*; WILEY-VCH Verlag GmbH&Co. (2006)
- [6] R. E. Booker, J. Sell; *The nanostructure of the cell wall of softwoods and its functions in a living tree*; Holz als Roh- und Werkstoff 56 (1998); 1-8
- [7] A. Wiedenhöft; *Structure and Function of Wood*; General Technical Report FPLGTR190 (08.01.2013)  
URL: [http://www.fpl.fs.fed.us/documnts/fplgtr/fplgtr190/chapter\\_03.pdf](http://www.fpl.fs.fed.us/documnts/fplgtr/fplgtr190/chapter_03.pdf)
- [8] D. Kretschmann; *Nature Materials: Velcro mechanics in wood*; Nature Materials 2 (2003); 775-776
- [9] A. Ebringerova, T. Heinze; *Naturally occurring xylans structures: Isolation procedures and properties*; Macromolecule Rapid Communication Volume 21 Issue 9 (2000); 542556
- [10] R. Frigg and S. Hartmann; *Models in Science* (28.08.2012);  
URL: <http://plato.stanford.edu/archives/fall2012/entries/models-science>
- [11] S.M. Notley, B. Pettersson, L. Wågberg, *Direct Measurement of attractive van der Waals forces between regenerated cellulose surfaces in an aqueous environment*, J.Am. Chem. Soc. 126 (2004); 13930-13931
- [12] F. Rehfeld, M. Tanaka; *Hydration forces in ultrathin films of cellulose*; Langmuir 19 (2003); 14671473
- [13] M. Roman; *Model Cellulosic Surfaces: History and Recent Advances*; ACS Symposium Series Volume 1019 (2009); 3-53
- [14] M. Djak, *Investigation of cellulose-hemicellulose films on Si/SiO<sub>2</sub> substrates by means of Polarization Modulation Fourier Transform Infrared Spectroscopy*, Master Thesis at University of Technology Graz (2011)
- [15] G. Fourche; *An overview of the basic aspects of polymer adhesion. Part I: Fundamentals*; Polymer Engineering and Science 35 (1995); 957-967

- [16] R. Schennach, U. Hirn, E. Horvath et al.; *A Model Approach to Understand the Fiber-Fiber Bond in Paper*; Progress in Paper Physics Seminar (2011); 211-213
- [17] U. Hirn, R. Schennach, F. Schmied; *Towards Quantification of Bonding Energy and Bonding Mechanisms Between Pulp Fibers*; 3<sup>rd</sup> ICC Sapporo (2012)
- [18] R. A. Serway, R. J. Beichner, J. W. Jewett; *Physics For Scientists and Engineers - Fifth Edition*, Fort Worth: Saunders College Publishing (2000)
- [19] B. N. J. Persson, C. Ganser F. Schmied et al.; *Adhesion of cellulose fibres in paper*; J. Phys.: Condens. Matter Volume 25 Number 4 (2013)
- [20] Paul-Scherrer Institut (PSI); *Spincoating* (28.08.2012);  
URL: [http://materials.web.psi.ch/Research/Thin\\_Films/Methods/Spin.htm?forprint](http://materials.web.psi.ch/Research/Thin_Films/Methods/Spin.htm?forprint)
- [21] E. Kontturi, P.C. Thüne, J.W. Niemantsverdriet; *Novel method of preparing cellulose model surfaces by spin coating*; Polymer 44 (2003); 3621-3625
- [22] A. Miletzky; *Adsorption of Xylans onto Softwood Kraft Pulp*; CD-Laboratory Meeting (05.07.2012)
- [23] Truger, *Kalibrieren der Zugmaschine*, Bachelor thesis (2011)
- [24] Engineering Statistics Handbook, *Normal Probability Plot* (03.09.2012), URL: <http://www.itl.nist.gov/div898/handbook/eda/section3/normprpl.htm>
- [25] G. Buttler; *Ein einfaches Verfahren zur Identifikation von Ausreißern* (25.09.2012);  
URL: <http://www.statistik.wiso.uni-erlangen.de/forschung/d0009.pdf>
- [26] Hans Lohninger, *Ausreißertest nach Grubbs* (18.12.2012);  
URL: [http://www.statistics4u.info/fundstat\\_germ/ee\\_grubbs\\_outliertest.html](http://www.statistics4u.info/fundstat_germ/ee_grubbs_outliertest.html)
- [27] W. Rohm, *Qualitätsmanagement und angewandte Statistik*, Skript HTL Saalfelden (2003)
- [28] C. Ganser, S. Rohm, R. Schennach, C. Teichert; *AFM-nanoindentation of pulp fibres and cellulose films*; CD-Laboratory Meeting (17.09.2012)
- [29] C. Ganser, U. Hirn, S. Rohm et al.; *Mechanical properties of swollen thin cellulose films and pulp fibers*; In preparation, to be submitted to *Holzforschung*
- [30] E. Gilli, A.E. Horvath, U. Hirn et al.; *Analysis of CMC attachment onto cellulosic fibres by infrared spectroscopy*, Cellulose 16 (2009); 825-832
- [31] D. Klemm, B. Philipp, U. Heinze; *Comprehensive Cellulose Chemistry, Volume 1*; Wiley-VCH (1998)
- [32] T. Kondo, C. Sawatari; *A Fourier transform infra-red spectroscopic analysis of the character of hydrogen bonds in amorphous cellulose*, Polymer 37 (1996); 393- 399
- [33] National Institute of Standards and Technology; *Chemistry Webbook* (18.06.2011),  
URL: <http://webbook.nist.gov/chemistry/>
- [34] infra:lit4 B. Hinterstoisser, L. Salmen; *Application of dynamic 2D FTIR to cellulose*; Vibration-Spectroscopy 22 (2000); 111-118
- [35] CC Info: Pflanzen FotoFotolabortechnik; *Technik - Wie funktioniert was?* (20.11.2012);  
URL: <http://www.elektronikinfo.de/technik.htm>

- [36] Berufsgenossenschaft Rohstoffe und chemische Industrie; *Dimetylsulfoxid (Labor)* (4.12.12),  
URL: [http://www.gischem.de/download/01\\_8-000067-68-5-000000\\_1\\_1\\_1.PDF](http://www.gischem.de/download/01_8-000067-68-5-000000_1_1_1.PDF)
- [37] O. Miskovic, F. J. Schmied, C. Teichert; *Surface characterization of cellulose films with atomic force microscopy*; CD-Laboratory Meeting (14.12.2010)
- [38] M. Klemm, *Festigkeit von Xylan unter dem Einfluss von  $CaCl_2$* , Bachelor Thesis at Technical University of Graz (2012)

# List of Figures

1.1	Model of the cell wall structure. The grey lines in the secondary wall layers represent idealized cellulose microfibrils [8]. . . . .	3
1.2	A schematic description of the microfibril. From the left to the right: Tree trunk, tissue structure, Cell walls, macrofibrils, microfibrils and molecules. [5] . . . . .	3
1.3	Structure of a cellulose molecule after [5] . . . . .	4
1.4	Molecular structure of xylan for soft- and hardwood [5] . . . . .	4
1.5	Schematic image of the model system and the test procedure. . . . .	5
1.6	Example for good (a) and bad (b) mechanical interlocking [15]. . . . .	6
1.7	Intra- and intermolecular hydrogen bonds in a cellulose molecule network. The bonds are marked with dotted lines [14]. . . . .	7
1.8	Explanation of the Coulomb interaction [18]. Opposite charged particles attract each other (top), same charged particles repel each other (bottom). . . . .	7
2.1	The main steps of the spin-coating process [20] . . . . .	9
2.2	( $\rightarrow$ ) Synthesization of TMSC out of cellulose. ( $\leftarrow$ ) Hydrolysis of TMSC to cellulose [21]. . . . .	10
2.3	Swelling of the films inside a vessel. . . . .	11
2.4	The arrangment inside the shelf drier. . . . .	11
2.5	Modified power rheometer . . . . .	12
2.6	Test procedure before the actual tensile test. The force F is illustrated with respect to the time t. . . . .	12
2.7	A sketch of a typical tensile-test result. The force F is plotted with respect to the length variation x. Included is the linear fit of the calibration. . . . .	13
2.8	Examples for Q-Q-plots: Left for normal distributed data, right for not normal distributed data [24]. . . . .	14
2.9	Schematic illustration of a nanoindentation experiment [28] . . . . .	16
2.10	The experimental procedure of an AFM nanoindentation experiment (left) and the experimental result (right) [28]. . . . .	17
3.1	Measured data and the linear fit for the calibration of the double sided cellotape. The force F is illustrated over the length variation x. . . . .	18
3.2	Reflection p-spectra of 4 random chosen cellulose samples. The spectra above are plotted over the whole wavenumber region, the figure below shows the results in the fingerprint region. Die dotted lines indicate the peaks at following positions (from right to left): 677, 858, 990, 1012, 1065, 1105, 1150, 1274 (blue), 2930, 3260, 3390 . . . . .	20
3.3	Reflection s-spectra of 4 random chosen cellulose samples. The spectra above are plotted over the whole wavenumber region, the figure below shows the results in the fingerprint region. Die dotted lines indicate the peaks at following positions (from right to left): 850, 980, 1010, 1048, 1107, 1147, 1192, 1249, 1274 (blue), 2875, 2952, 3240, 3620 . . . . .	21

3.4	The reflection p-spectra of the 4 samples at the wavenumber range of the $CH_2$ bending absorption. . . . .	24
3.5	AFM images of the film before (left) and after swelling (right). The axes are scaled in $\mu\text{m}$ . . . . .	25
3.6	Illustration of a detaching process during a tensile test. a) Connected films. b) Sample gets stretched. One films starts to go adrift. c) The detaching process continues, while the films themselves are still connected. d) Films disconnect. . . . .	27
3.7	Microscopic image of a detached film. . . . .	27
3.8	A tensile test example for an unbonding in the pressure period. The force $F$ (N) versus the length variation $x$ (mm) is illustrated. . . . .	27
3.9	Illustration of the invalid test marked with <sup>5</sup> . . . . .	28
3.10	A Q-Q plot of the cellulose-cellulose results. The maximum strength $F_{max}$ (blue crosses) is plotted with respect to the normal distribution. The red line represents perfect normal distributed data. . . . .	28
3.11	Valid tensile tests of cellulose films swelled in distilled water. The strength of the bonds $F$ (N) is plotted in respect to the length variation $x$ (mm). From the top to the bottom: Test series 1, test series 3, test series 5 and test series 6. . . . .	30
3.12	Comparison of the hardness of cellulose before (left) and after (right) swelling. . . . .	32
3.13	Profile across a hole in a film after the tensile test measured with an AFM. . . . .	33
3.14	An example of the strength crossing the zero newton line into the pressure area. The force $F$ (N) is illustrated versus the length variation $x$ (mm). . . . .	34
3.15	A Q-Q plot of the in ionic water swelled cellulose samples. The maximum strength $F_{max}$ (blue crosses) is plotted with respect to the normal distribution. The red line represents perfect normal distributed data. The incircled data points indicate possible outliers. . . . .	34
3.16	Valid tensile tests of the in ionic water swelled cellulose samples. The strength of the bonds $F$ (N) is plotted in respect to the length variation $x$ (mm). From the top to the bottom: Test series 1, test series 2 and test series 3. . . . .	36
3.17	Comparison of cellulose swelled in distilled with cellulose swelled in ionic water. On the left the maximum strength $\bar{F}_{max}$ (N). On the right the bonding energy $\bar{E}_b$ ( $\frac{kJ}{mm^2}$ ). . . . .	37
3.18	Four different microscope images of different cellulose films swelled in ionic water after the tensile test. The green and yellow background is due to the cellulose, the black lines in front are salt. . . . .	38
3.19	Illustration of the gap between the films due to the deposition of salt. . . . .	38
3.20	Comparison of the hardness $H$ (left) and the reduced modulus $E_r$ (right) of a cellulose films swelled in distilled water and in ionic water. . . . .	39
3.21	Schematic image of salt solved in water [35]. . . . .	39
3.22	Structure of dimetyl sulfoxide (DMSO) [?] . . . . .	40
3.23	Microscopic images of the cellulose surface before (left) and after (right) spin-coating with DMSO at two different striking spots. . . . .	41
3.24	Valid tensile tests of, with DMSO spincoated, cellulose samples. Not included: Invalid test one. . . . .	42
3.25	The comparison of cellulose with cellulose spincoated with DMSO. Right, the maximum strength $F_{max}$ . Left, the bonding energy $E_b$ . Both are swelled in distilled water. . . . .	43
3.26	A Q-Q plot of the xylan samples swelled in distilled water. The results for the maximum strength $F_{max}$ (blue crosses) are plotted with respect to theoretical normal quantile. The red line represents perfect normal distributed data. The incircled data point indicates a possible outlier. . . . .	44

3.27	Valid tensile tests of xylan films swelled in distilled water. The force $F$ (N) is plotted in respect to the length variation $x$ (mm). Top-down: Test series 1, test series 2, test series 3. . . . .	46
3.28	The hardness of the cellulose films is compared to hardness of the xylan films. Left in the dry state, right in the wet state. . . . .	47
3.29	Comparison of the maximum strength $F_{max}$ (N) (right) and the bonding energy $E_b$ ( $\frac{kJ}{nm^2}$ ) of xylan with cellulose (left). Both results are obtained for swelling in distilled water. . . . .	48
3.30	A Q-Q plot of the mixed samples swelled in distilled water. The blue crosses ( $F_{max}$ ) are the experimental results, the red line represents perfect normal distributed data. . . . .	49
3.31	Valid tensile tests of the in distilled water swelled cellulose-xylan samples. The force $F$ (N) is plotted in respect to the length variation $x$ (mm). Top-down: Test series 2 and 3. . . . .	51
3.32	Comparison of the results for cellulose and xylan swelled in distilled water, with the results obtained for mixed samples. The left histogram shows the values for the maximum strength $F_{max}$ , the right one for the bonding energy $E_b$ . . . .	51
3.33	Q-Q plot of the xylan+DMSO samples. The maximum strength $F_{max}$ (blue crosses) is plotted in respect to the theoretical normal quantile. The red line indicates perfect normal distributed data. . . . .	53
3.34	Valid tensile tests of the in distilled water swelled xylan+DMSO samples. The force $F$ (N) is plotted in respect to the length variation $x$ (mm). . . . .	54
3.35	Comparison of xylan with xylan+DMSO, both swelled in distilled water. Left the maximum strength $F_{max}$ , right the bonding energy $E_b$ . . . . .	54
3.36	Hardness-Comparison of a xylan-film with a xylan-DMSO film . . . . .	55
3.37	Q-Q plot of xylan sample swelled in water containing $CaCl_2$ . The results for the maximum strength $F_{max}$ (blue crosses) are plotted in respect to the theoretical normal quantile. The red line is representing perfect normal distributed data. . .	57
3.38	Valid tensile tests of the xylan films swelled in water containing $CaCl_2$ . Top-bottom: Tests 1-7 and 8-14 of the second test series. . . . .	58
3.39	Comparison of xylan swelled in distilled water with xylan swelled in ionic water. Left, the maximum strength $F_{max}$ (N), right the bonding energy $E_b$ ( $\frac{kJ}{nm^2}$ ) . . . .	58
3.40	Hardness comparison of xylanfilms swelled in distilled and swelled in ionic water. . . . .	59
3.41	Illustration of possible Coulomb interactions between two xylan films swelled in $CaCl_2$ water. a) Repulsive configuration; b) Attractive configuration . . . . .	60

# List of Tables

3.1	Fit of the the strength curves in the linear range. . . . .	19
3.2	Absorptionpeaks of cellulose. The measured values (Experiment) are compared to literaturevalues (Literature) and to values obtained for same produced cellulose-films at the same interferometer(Reference). Most of the literature data is abstracted from [31]. The reference data is recorded in [14]. . . . .	23
3.3	Integrated area in the range of 2800-3000 $cm^{-1}$ and the resulting film thickness.	24
3.4	Thickness of the Film in the dry and the wet state, measured with an AFM. . .	25
3.5	Tensile test results for cellulose samples swelled in distilled water. . . . .	26
3.6	Valid tensile tests results for cellulose films swelled in distilled water. . . . .	29
3.7	Results of the nanointentation test . . . . .	31
3.8	AFM investigation of two films before and after the tensile test. . . . .	32
3.9	Tensile test results for cellulose swelled in water containing $CaCl_2$ . . . . .	33
3.10	Valid tensile test results for cellulose swelled in water containing $CaCl_2$ . . . . .	35
3.11	Tensile test results of cellulose samples spincoated with DMSO. . . . .	42
3.12	Tensile test results for xylan swelled in distilled water. . . . .	43
3.13	Valid tensile test results for xylan films swelled in distilled water . . . . .	45
3.14	Nanoindentation test results for xylan. . . . .	47
3.15	Tensile tests results for cellulose-xylan samples (mixed samples) swelled in distilled water. . . . .	48
3.16	Valid tensile test results for the mixed samples swelled in distilled water. . . . .	50
3.17	Tensile test results for xylan with stored DMSO swelled in distilled water (xylan+DMSO). . . . .	52
3.18	Tensile test results for xylan films swelled in ionic water. . . . .	56
4.1	Results of the tensile tests . . . . .	62
4.2	Nanoindenation results of different film settings . . . . .	63

# Appendix A

## Analysis with Matlab

```
% Analysis of the Tensile Test Results for Cellulose swelled in distilled Water
```

```
clear all
close all
clc
```

```
k= [1:22]; %Number of valid Tensile test results
```

```
kmax =length(k);
```

```
for n= 1:kmax
```

```
nr= k(n);
name=['probe',num2str(nr),'.csv']; %Loading the tensile test data
A=csvread(name);
t= A(:,1); %Time of test
h= A(:,2); %Length Variation x
F= A(:,3); %Strength F
```

```
% Evalutaion of the Maximum Strength (since negative Force--> min)
F_max(n)= min(F);
```

```
% Evulation of the Bonding Energy-----
```

```
% to cut of the noise, -0.01 is the boundary
```

```
F_E= F(F<-0.01);
```

```
h_E= h(F<-0.01);
```

```
h_E = h_E-h_E(1); %Every curve starts at 0
```

```
%An approximation of the integral of F(h) via the trapezoidal method
```

```
E(n) = trapz (F_E, h_E);
```

```
%Subtraction of the Calibration F= (k*x + d)-----
```

```
k= -49.6; %Slope of the Fit
```

```

d= 0.21;    %x-Value for F = ON

%Length variation of the cellotapes at F_max (h= F_max -d)/ k
h_cal = (F_max(n) - d)/k;
% By the Cellotapes absorbed energy E = int(F*dx) = k*x^2/2 + k*x
E_Cal(n) = k* h_cal^2/2 + d*h_cal;
%Bonding Energy
E_b(n) = E(n) - E_Cal(n);

%Plot-----
figure(1)
hold on
plot(h_E,F_E)

end
xx=linspace (0,0.1,10);
yy= k*xx+ d;
plot(xx,yy,'r')
xlabel('Length Variation x / mm')
ylabel('Strength F / N')
hold off

%Q-Q-Plot of the maximum Strength results (Outliers included)
figure(2)
qqplot(F_max)

%Outliertest after Grubb-----

F_mean= mean(F_max);
F_var = var(F_max);    %Mean-value variance, and standard deviation
F_std = std(F_max);

for n= 1:kmax

    %G = max |F - F_mean| / standard deviation
    G= max( abs(F_max- F_mean))/ F_std;

    anz = kmax-(n-1); %Number of remaining compounds
    a=0.05;          %Signifikance Level

    t = tinva/(2*anz),anz-2); %Inverse t-Distribution

    %Critical Value gc
    gc = (anz - 1) / sqrt(anz) * sqrt(t^2 / (anz - 2 + t^2));

    % if G > gc, then this Value is an Outlier, and the procedure is repeated
    if G > gc

        fprintf (' Outlier indentified \n')

```

```

% Deleting of these value out of the results
F_max (abs(F_max-F_mean) == max (abs(F_max-F_mean))) = 0;
E= E (F_max ~= 0 );
E_call1 = E_call1( F_max ~= 0) ;
F_max = F_max (F_max ~= 0);

%New mean Value, variance and standard deviation
F_mean = mean(F_max);
F_var = var (F_max);
F_std = std (F_max);

% if G< gc, then this value is not outlier
% Grubb-test is over
else

    fprintf (' Kein Außreißer mehr ')
    break
end

end

%Q-Q-Test with outlier(s) not included
figure(3)
qqplot(F_max)

%Mean-value and variance of the Energy
E_mean = mean (E_b);
E_var= var (E_b);
E_std = std(E_b);

%Saving of the results
F_max=F_max';
E_b = E_b';
save('F.txt', 'F_max', '-ASCII');
save('E.txt', 'E_b', '-ASCII');

```